SIAM J. APPL. MATH.
Vol. 73, No. 1, pp. 493–522

RETRIEVAL OF A GREEN'S FUNCTION WITH REFLECTIONS FROM PARTLY COHERENT WAVES GENERATED BY A WAVE PACKET USING CROSS CORRELATIONS*

MAARTEN V. DE HOOP†, JOSSELIN GARNIER‡, SEAN F. HOLMAN†, AND KNUT SØLNA§

Abstract. We analyze the "field-field" cross correlation associated with partly coherent scattered waves generated by a wave packet. The configuration consists of a slab in which random medium fluctuations occur; the bottom of the slab is bounded by a deterministic discontinuity (a smooth reflector). Following the dyadic parabolic scaling of wave packets, and scaling the random fluctuations appropriately, we arrive at a description in terms of a system of linear Itô–Schrödinger diffusion models. Studying the Wigner distributions of the fields generated by these models leads to a "blurring" transformation, providing a complete characterization of the cross correlation. We obtain a description of the cross correlation in terms of this transformation applied to the effective transmission operator that arises as a solution of the Itô–Schrödinger model. Most of the analysis is focussed on the interaction of the deterministic reflector with the random fluctuations through the waves in the regime of fine scales.

Key words. wave propagation, Green's function, estimation, cross correlation, random medium

AMS subject classifications. 35R60, 60B12, 86A15

DOI. 10.1137/110836286

1. Introduction.

We analyze the "field-field" cross correlation associated with partly coherent waves generated by a wave packet and observed at a pair of distinct receivers embedded within a random medium. The result is a Green's function estimate which captures both the high-frequency body wave reflections and the scattering due to the random fluctuations of the medium.

As a model configuration, we consider a slab in which random medium fluctuations occur. The bottom of the slab is bounded by a deterministic discontinuity (a smooth reflector). We consider waves incident from above the slab and place our receivers within the slab to study the cross correlations between them. We assume that the deterministic component of the medium is constant within the slab and that the slab is flat.

The waves are excited by a wave packet. The wave packet contains a particular scale, which is selected in relation to the scale of the random fluctuations of the medium within the slab. Through localization in phase space, the propagation and scattering of a wave packet can be described by a coupled system of paraxial wave equations. The accuracy of this description can be proven to improve with increasingly finer scales, which is the regime considered here. Indeed, we view the cross correlations

*Received by the editors June 2, 2011; accepted for publication (in revised form) October 5, 2012; published electronically February 26, 2013. This work was partially supported by the Mathematical Sciences Research Institute Fall Program 2011 on Inverse Problems and Applications, and by NSF ARRA grant DMS 0908274 and ERC Advanced Grant Project MULTIMOD-267184.
http://www.siam.org/journals/siap/73-1/83628.html

†Center for Computational and Applied Mathematics, Purdue University, West Lafayette, IN 47907 (mdehoop@math.purdue.edu, sfholman@math.purdue.edu).

‡Laboratoire de Probabilités et Modèles Aléatoires & Laboratoire Jacques-Louis Lions, Université Paris 7, site Chevaleret, case 7012, 75205 Paris Cedex 13, France (garnier@math.jussieu.fr).

§Department of Mathematics, University of California at Irvine, Irvine, CA 92697-3875 (ksolna@math.uci.edu).

in the context of parametrix constructions. The paraxial form of the system allows for the use of Itô's stochastic calculus (for Hilbert-space valued processes) to analyze the scattering due to the random fluctuations; indeed, it enables the closure of the hierarchy of moment equations.

The solution procedure of each coupled system of paraxial wave equations is based on an invariant embedding-type approach, generating a transmission and a reflection operator that capture the scattering due to the random fluctuations in the medium. Thus we arrive at a coupled system of Riccati equations for the mentioned operator kernels. In the limit of fine scales (high "frequency"), we then obtain a decoupled system of linear Itô–Schrödinger equations for formally limiting transmission and reflection operator kernels. We remark that the kernels themselves do not in general converge; however, the associated wave fields converge weakly as described in Proposition 4.1 below. The Itô–Schrödinger equations can be viewed as a generalization of the paraxial equations associated with a wave packet. By combining wave packets and the relevant solutions to the Itô–Schrödinger equations, we can generate general sources and the corresponding waves.

The solutions to the Itô–Schrödinger equations allow us to calculate the statistics of the transmitted and backscattered fields and analyze the cross correlations. Indeed, we find that the cross correlation of the wave field between two points has four primary contributions corresponding to waves directly transmitted through the two points and those reflected. Each of these contributions can be represented as a filter with a self-averaging property applied to the transmission operator arising from the Itô–Schrödinger equations. We estimate these filters in particular scaling regimes by analyzing Wigner distributions and thus obtain a description of the cross correlation in terms of a transformation applied to the transmission operator. The transformation represents diffusion or blurring. Essentially, by synthesizing a wave packet source and "field-field" cross correlation, we succeed in estimating a Green's function from noisy reflections in the high-frequency regime. We explicitly characterize the reflections in the case of small offsets between the two detectors using the mentioned transformations in the strongly cluttered regime. Locally transverse medium diversity aids in sharpening these tranformations, while the wave packets accommodate uncertainty in phase space.

In the past decade, the question of how cross correlations between diffuse fields can capture the Green's function has been an important topic of research [20, 27]. Much of this work is based on exploiting ambient noise sources. The idea of using ambient noise for the retrieval of a body-wave reflection response, in a planarly layered medium, dates back to Claerbout [3]. He also conjectured that, in general media, cross-correlating ambient noise traces from two locations recaptures the wave field at one of the locations, excited by a point source at the other location. This led to much work on so-called interferometric imaging techniques, which exploit wave coherence for imaging purposes; we refer the reader to the review papers [22, 24] for a general exposition and further references. An early example of a field application was reported by Scherbaum [15], who analyzed auto-correlations of recordings of low-magnitude earthquakes and generated *pseudoreflection seismograms*. The cross correlation method has also been developed in helioseismology [7]. Cross-correlating (diffuse) coda waves [2] and ambient seismic noise [16, 17] have been shown to result in the retrieval of surface waves observed at one station and excited at the other station [28]. Furthermore, *turning* body waves have been observed in cross-correlating ambient noise [13]; in an exploration seismology setting, *reflected* body waves have also

been recovered by cross correlations [6]. A study of point diffraction, in the absence of random medium fluctuations, but with a closed surface of point sources, in terms of the optical theorem, was given in [23]. The retrieval of direct and reflected body waves using a teleseismic (S-wave) coda was discussed in [19]. In [26] Ward identities were used to identify relations between correlations of (diffuse) fields and Green's functions for rather general systems including systems with nonlocal constitutive relations. Integral equations that relate wave field correlations to Green's functions were derived from reciprocity relations and presented in [21], including cases with partial aperture and nonequipartition or nondiffusive situations.

Here we show how Claerbout's conjecture applies to the situation when we use a single source in terms of a deterministic wave packet located over a cluttered medium modeled as a random field. The regime is that of the paraxial approximation with a parabolic scaling and a narrow wave beam, and therefore it is different from the diffusive case. We show that the cross correlation gives an estimate of the Green's function and that the estimate is enhanced by the medium clutter. We characterize explicitly how the resolution in the estimate relates to the statistical properties of the random field modeling the medium clutter. Our approach is to explicitly model the statistical structure of the medium microscale and show how this can be seen as increasing the "effective source aperture" via increased wave diversity caused by the scattering from the microstructure. We stress here that we obtain an approximation of the full (random) Green's function modified via a convolution with a kernel or filter that is deterministic in the scaling limit that we consider. The support of the filter gives the accuracy of the estimation which can be enhanced by the clutter. This representation is similar to the one obtained in [25] in the nonrandom, but limited aperture, case, and one could envision using a deconvolution technique as in [25] to compensate for the smearing we obtain here.

The exploitation of a scattering medium for capturing the Green's function by the "field-field" cross correlation in the case with ambient noise was studied in [5, 10]. We remark here that the mathematical analysis of the "field-field" cross correlation in this setting from the point of view of stochastic calculus has just begun [1, 10, 4]. Finally, the framework analyzed here is related to the so-called "virtual source method" that recently has come to play an important role in geophysics, where a heterogeneous overburden "creates a noise field" impinging on imbedded receivers such that the associated cross correlations and Green's function estimates can be exploited for deep imaging; see [9] and references therein. There, in particular, the case with strong medium fluctuations and wide aperture is considered in the case of layered microstructure, as opposed to the narrow angle configuration considered here that is associated with the paraxial formulation. The analysis in the wide angle case involves a stationary phase approximation to identify the main contributions of the correlations; this is the case also in [18], where a constant or smooth background is considered.

2. Scaling and assumptions. We study the acoustic wave equation with a forcing term:

$$\frac{\partial^2 p}{\partial t^2}(t,z,\boldsymbol{x}) - c^2(z,\boldsymbol{x})\Delta p(t,z,\boldsymbol{x}) = -\chi_\epsilon(t,\boldsymbol{x})\,\delta'(z), \tag{2.1}$$

where $t \in \mathbb{R}$, $(z,\boldsymbol{x}) \in \mathbb{R}\times\mathbb{R}^d$, and the Laplacian is taken in all of the spatial variables $(z,\boldsymbol{x})$. We distinguish z as the special direction along which our waves will propagate.

The wave speed $c(z,\boldsymbol{x})$ of the randomly heterogeneous medium is assumed to be

$$c^2(z,\boldsymbol{x}) = \begin{cases} 1 & \text{if } z > 0, \\ 1+\varepsilon^3\nu(\frac{z}{\varepsilon^2},\frac{\boldsymbol{x}}{\varepsilon^2}) & \text{if } -L < z \le 0, \\ c_0^2 & \text{if } z \le -L \end{cases}$$

for constants L and $c_0 > 0$. Here ν is a zero-mean, stationary random field with correlation length and standard deviation of order one, which represents the random fluctuations in the medium. Note that we have introduced dimensionless coordinates so that that the velocity in the positive half-space is unity; thus time and space variables can be contrasted in terms of their relative magnitude. We write next

$$C(z,\boldsymbol{x}) = \mathbb{E}[\nu(z'+z,\boldsymbol{x}'+\boldsymbol{x})\nu(z',\boldsymbol{x}')], \tag{2.2}$$

$$D(\boldsymbol{x}) = \int_{-\infty}^{\infty} C(z,\boldsymbol{x})\,dz. \tag{2.3}$$

We also assume that ν satisfies strong mixing conditions in z.

The forcing functions $\chi_\epsilon(t,\boldsymbol{x})$ are given by $\chi_\epsilon(t,\boldsymbol{x}) = \chi(\varepsilon^{-4}t,\varepsilon^{-2}\boldsymbol{x})$, where χ is the real part of a function whose Fourier transform in both t and $\boldsymbol{x}$ has support contained in the box $[1/2,2]_\omega \times [-1/\sqrt{2},1/\sqrt{2}]^d_{\boldsymbol{\kappa}}$; recall here that we have introduced dimensionless coordinates. Our conventions and notation for the Fourier transform are

$$\chi(t,\boldsymbol{x}) = \frac{1}{(2\pi)^{d+1}}\iint \hat\chi(\omega,\boldsymbol{\kappa})\,e^{-i(\omega t-\boldsymbol{\kappa}\cdot\boldsymbol{x})}\,d\omega d\boldsymbol{\kappa} = \frac{1}{2\pi}\int \check\chi(\omega,\boldsymbol{x})\,e^{-i\omega t}\,d\omega,$$

$$\hat\chi(\omega,\boldsymbol{\kappa}) = \iint \chi(t,\boldsymbol{x})e^{i(\omega t-\boldsymbol{\kappa}\cdot\boldsymbol{x})}\,dtd\boldsymbol{x}, \qquad \check\chi(\omega,\boldsymbol{x}) = \int \chi(t,\boldsymbol{x})e^{i\omega t}\,dt.$$

What we have in mind here is that χ_ϵ represents the real part of a wave packet at scale k with $2^k = \varepsilon^{-4}$ oriented in the t "direction." The important aspect here is the special scalings of the source (with spatial radius of order ε^2 and time pulse width of order ε^4) which supports the paraxial regime and not its specific shape.

This scaling with ε is consistent with the paraxial regime, which will be discussed in the next section, inasmuch as solutions of (2.1) with $\nu = 0$ may be approximated up to an error of order ε^4 (this error would in general be only of order ε^2 if there were a nonconstant background) by the solution of a decoupled system of paraxial equations. We point out the important aspects of the scaling:

- The transverse width, R_0, of the source function is of order ε^2.
- The correlation length or radius of the fluctuations is of the same order as R_0; this regime guarantees nontrivial interaction between the fluctuations of the medium and the waves.
- The propagation distance L, is of order one; thus the ratio between the propagation distance and the correlation length of the fluctuations of the medium is of order ε^{-2}.
- The amplitude ε^3 of the fluctuations of the medium is chosen so that the impact of these fluctuations will be of order one when ε goes to zero. That is, if the magnitude of the fluctuations were smaller than ε^3, then the wave would propagate as if the medium were homogeneous, while if the order of magnitude were larger, then the wave would not penetrate the slab at all.

The objective here is to study how the random fluctuations affect observations (and, in particular, cross correlations) of the solution p to (2.1) as $\varepsilon \to 0$, which represents the high-frequency limit. Our main scaling assumption is thus the following.

ASSUMPTION 1. $\varepsilon \ll 1$.

Note that, in a multiscale framework, there may be additional random fluctuations in the medium with small correlation lengths (i.e., smaller than ε^2), but they do not play any role, provided that their amplitude is still of the order of ε^3. This can be seen from the expression of the covariance function of the Brownian field that models the cumulative effect of the random fluctuations of the medium in Proposition 4.1 and that is proportional to the integrated covariance of the random fluctuations. As a result the components of the random fluctuations of the medium with small correlation lengths average out. In fact, if the random fluctuations of the medium have only components with a small correlation length (smaller than ε^2) and an amplitude of the order of ε^3, then their effect is negligible in the asymptotic framework $\varepsilon \to 0$. Small-scale random fluctuations can be effective only if their amplitude is larger. For instance, if the correlation length of the random fluctuations of the medium is of order ε^4, then the interaction with the waves is effective if the amplitude of the fluctuations is of order ε^2, and this interaction is then captured by the radiative transport equation [14].

We finally note that the scaling considered in this paper is relevant in a geophysical context. In this case we may think that the propagation distance is on the order of 10–100 kilometers, the wavelength is on the order of 10–100 meters, and the correlation length (and the array size) is on the order of 0.1–1 kilometer. This scaling regime can also be relevant to modeling laser beam propagation through the atmosphere. In this case the propagation distance is on the order of 1 kilometer, the correlation length (and the beam width) is on the order of 1–10 centimeters, and the wavelength is on the order of 1 micrometer.

3. Coupled system of paraxial equations and transmission and reflection operators.

3.1. Totally deterministic case. In this subsection we consider only the totally deterministic case corresponding to $\nu = 0$ in (2.1), so that the wave speed depends only on z, $c(z, \boldsymbol{x}) \equiv c(z)$ with $c(z) = 1$ for $z > -L$, and $c(z) = c_0$ for $z < -L$. We provide precise estimates of how well the solutions of (2.1) can be approximated by solutions of a decoupled system of paraxial equations (i.e., show that we are in the paraxial regime). Also, we study the transmitted and reflected wave fields in the high-frequency limit, which is the deterministic version of Proposition 4.1.

To begin, we convert (2.1) to an equivalent system which distinguishes z in a more transparent way. Indeed, if p^{D} is a solution of (2.1), then we have a corresponding solution of the system

$$\frac{\partial}{\partial z}\begin{pmatrix} p^{\mathrm{D}} \\ v^{\mathrm{D}} \end{pmatrix} = \begin{pmatrix} 0 & 1 \\ \frac{1}{c(z)^2}\frac{\partial^2}{\partial t^2} - \Delta_{\boldsymbol{x}} & 0 \end{pmatrix}\begin{pmatrix} p^{\mathrm{D}} \\ v^{\mathrm{D}} \end{pmatrix} + \begin{pmatrix} 0 \\ \chi_\epsilon(t, \boldsymbol{x})\, \delta'(z) \end{pmatrix}, \tag{3.1}$$

where $\Delta_{\boldsymbol{x}}$ is the transverse Laplacian. On the other hand, if p^{D} and v^{D} are solutions of (3.1) on $z \notin \{0, -L\}$ satisfying the jump conditions

$$p^{\mathrm{D}}(t, 0^+, \boldsymbol{x}) - p^{\mathrm{D}}(t, 0^-, \boldsymbol{x}) = \chi_\epsilon(t, \boldsymbol{x}) \quad \text{and} \quad v^{\mathrm{D}}(t, 0^+, \boldsymbol{x}) - v^{\mathrm{D}}(t, 0^-, \boldsymbol{x}) = 0, \tag{3.2}$$

and continuous across $z = -L$, then p^{D} is also a solution of (2.1).

We find solutions of (3.1) by diagonalizing the matrix operator on the right-hand side microlocally. Indeed, let $\lambda(\omega,\boldsymbol{\kappa}) = \sqrt{\omega^2 - |\boldsymbol{\kappa}|^2}$,

$$\mathcal{Q}(\omega,\boldsymbol{\kappa}) = \begin{pmatrix} \lambda^{-\frac{1}{2}} & \lambda^{-\frac{1}{2}} \\ i\,\lambda^{\frac{1}{2}} & -i\,\lambda^{\frac{1}{2}} \end{pmatrix}, \quad \text{and} \quad \mathcal{Q}^{-1}(\omega,\boldsymbol{\kappa}) = \frac{1}{2}\begin{pmatrix} \lambda^{\frac{1}{2}} & -i\,\lambda^{-\frac{1}{2}} \\ \lambda^{\frac{1}{2}} & i\,\lambda^{-\frac{1}{2}} \end{pmatrix}.$$

It is straightforward to check that the unique solution to (3.1) on $\{-L < z < 0\}$ with $p^{\mathrm{D}}(t,0^-,\boldsymbol{x}) = \varphi_p(t,\boldsymbol{x})$ and $v^{\mathrm{D}}(t,0^-,\boldsymbol{x}) = \varphi_v(t,\boldsymbol{x})$ is given by

$$\begin{pmatrix} p^{\mathrm{D}}(\cdot,z,\cdot) \\ v^{\mathrm{D}}(\cdot,z,\cdot) \end{pmatrix} = \mathcal{P}^{\mathrm{D}}(z)\begin{pmatrix} \varphi_p \\ \varphi_v \end{pmatrix}, \tag{3.3}$$

provided that the support of the Fourier transforms of φ_p and φ_v is compactly contained in the region $\{|\omega| > |\boldsymbol{\kappa}|\}$, where the (deterministic) propagator is defined by

$$\mathcal{P}^{\mathrm{D}}(z)\begin{pmatrix} \varphi_p \\ \varphi_v \end{pmatrix} := \mathcal{Q}(D_t,D_{\boldsymbol{x}})\begin{pmatrix} e^{i\,z\lambda(D_t,D_{\boldsymbol{x}})} & 0 \\ 0 & e^{-i\,z\lambda(D_t,D_{\boldsymbol{x}})} \end{pmatrix}\mathcal{Q}^{-1}(D_t,D_{\boldsymbol{x}})\begin{pmatrix} \varphi_p \\ \varphi_v \end{pmatrix}. \tag{3.4}$$

We specify φ_p and φ_v by invoking a directional decomposition of the wave field and requiring that there be no incoming waves from the top half-space $\{z > 0\}$ or from the bottom half-space $\{z < -L\}$. Indeed, let us suppose that p^{D} and v^{D} are our solutions of (3.1), and introduce the following directional decomposition:

$$\begin{pmatrix} a^{\mathrm{D}}(\cdot,z,\cdot) \\ b^{\mathrm{D}}(\cdot,z,\cdot) \end{pmatrix} := \begin{pmatrix} e^{-i\,z\,\lambda(D_t,D_{\boldsymbol{x}})} & 0 \\ 0 & e^{i\,z\,\lambda(D_t,D_{\boldsymbol{x}})} \end{pmatrix}\mathcal{Q}^{-1}(D_t,D_{\boldsymbol{x}})\begin{pmatrix} p^{\mathrm{D}}(\cdot,z,\cdot) \\ v^{\mathrm{D}}(\cdot,z,\cdot) \end{pmatrix}. \tag{3.5}$$

The first component (a^{D}) of the decomposition is the portion of the wave field traveling in the positive z direction (up), while the second component (b^{D}) is the portion traveling in the negative z direction (down). We ask that there be no incoming waves, which thus means

$$b^{\mathrm{D}}(t,0^+,\boldsymbol{x}) = 0 \quad \text{and} \quad a^{\mathrm{D}}(t,-L^-,\boldsymbol{x}) = 0.$$

Using these conditions as well as (3.2), we obtain

$$\begin{aligned} a^{\mathrm{D}}(t,0^+,\boldsymbol{x}) &= a^{\mathrm{D}}(t,0^-,\boldsymbol{x}) + \frac{\sqrt{\lambda(D_t,D_{\boldsymbol{x}})}}{2}\chi_\varepsilon(t,\boldsymbol{x}), \\ b^{\mathrm{D}}(t,0^-,\boldsymbol{x}) &= -\frac{\sqrt{\lambda(D_t,D_{\boldsymbol{x}})}}{2}\chi_\varepsilon(t,\boldsymbol{x}), \\ a^{\mathrm{D}}(t,-L^+,\boldsymbol{x}) &= e^{2\,i\,L\lambda(D_t,D_{\boldsymbol{x}})}\,\mathcal{R}^{\mathrm{D}}(D_t,D_{\boldsymbol{x}})\,b^{\mathrm{D}}(t,-L^+,\boldsymbol{x}), \\ b^{\mathrm{D}}(t,-L^-,\boldsymbol{x}) &= \mathcal{T}^{\mathrm{D}}(D_t,D_{\boldsymbol{x}})\,b^{\mathrm{D}}(t,-L^+,\boldsymbol{x}), \end{aligned}$$

where $\mathcal{R}^{\mathrm{D}}$ and $\mathcal{T}^{\mathrm{D}}$ are the frequency-dependent reflection and transmission operators of the interface at $z = -L$:

$$\mathcal{R}^{\mathrm{D}}(\omega,\boldsymbol{\kappa}) = \frac{c_0 - l_0(\omega,\boldsymbol{\kappa})}{c_0 + l_0(\omega,\boldsymbol{\kappa})}, \quad \mathcal{T}^{\mathrm{D}}(\omega,\boldsymbol{\kappa}) = 2\frac{\sqrt{c_0\,l_0(\omega,\boldsymbol{\kappa})}}{c_0 + l_0(\omega,\boldsymbol{\kappa})},$$
$$\text{and} \quad l_0(\omega,\boldsymbol{\kappa}) = \sqrt{\frac{\omega^2 - c_0^2|\boldsymbol{\kappa}|^2}{\omega^2 - |\boldsymbol{\kappa}|^2}}.$$

By (3.2) and all of these conditions, we have

$$p^{\mathrm{D}}(t,-L^-,\boldsymbol{x}) = -\frac{1}{2}e^{i\,L\,\lambda(D_t,D_{\boldsymbol{x}})}\mathcal{T}^{\mathrm{D}}(D_t,D_{\boldsymbol{x}})\chi_\varepsilon(t,\boldsymbol{x}),$$
$$p^{\mathrm{D}}(t,0^+,\boldsymbol{x}) = -\frac{1}{2}e^{2\,i\,L\lambda(D_t,D_{\boldsymbol{x}})}\mathcal{R}^{\mathrm{D}}(D_t,D_{\boldsymbol{x}})\chi_\varepsilon(t,\boldsymbol{x}) + \frac{1}{2}\chi_\varepsilon(t,\boldsymbol{x}).$$

Now we may establish the following elementary result about high-frequency transmission and reflection of the wave field.

THEOREM 3.1. *The pair* $(p^{\mathrm{D}}(L+\varepsilon^4 t,-L^-,\varepsilon^2\boldsymbol{x}),\ p^{\mathrm{D}}(2L+\varepsilon^4 t,0^+,\varepsilon^2\boldsymbol{x}) - 1/2\chi(2L/\varepsilon^4+t,\boldsymbol{x}))$ *converges in* $C^0(\mathbb{R}_t,L^2(\mathbb{R}^d_{\boldsymbol{x}},\mathbb{R}^2))\cap L^2(\mathbb{R}_t,L^2(\mathbb{R}^d_{\boldsymbol{x}},\mathbb{R}^2))$ *to* $(p^{\mathrm{D}}_{\mathrm{T}}(t,\boldsymbol{x}),$ $p^{\mathrm{D}}_{\mathrm{R}}(t,\boldsymbol{x}))$ *as* $\varepsilon\to 0$, *where*

$$p^{\mathrm{D}}_{\mathrm{T}}(t,\boldsymbol{x}) = -\frac{\mathcal{T}_0}{2}e^{-i\,L\,\frac{|D_{\boldsymbol{x}}|^2}{2D_t}}\chi(t,\boldsymbol{x}),\qquad p^{\mathrm{D}}_{\mathrm{R}}(t,\boldsymbol{x}) = -\frac{\mathcal{R}_0}{2}e^{-i\,L\,\frac{|D_{\boldsymbol{x}}|^2}{D_t}}\chi(t,\boldsymbol{x}), \tag{3.6}$$

and

$$\mathcal{T}_0 = 2\frac{c_0^{1/2}}{c_0+1},\qquad \mathcal{R}_0 = \frac{c_0-1}{c_0+1}. \tag{3.7}$$

Proof. Note that the support of $\hat{\chi}_\varepsilon$ is contained in (for ε sufficiently small) the set $\{\omega\geq|\boldsymbol{\kappa}|^2\}\cap\{\omega>1/(2\varepsilon^4)\}$. Thus $l_0(\omega,\boldsymbol{\kappa})\to 1$ and $\lambda(\omega,\boldsymbol{\kappa})-(\omega-\frac{|\boldsymbol{\kappa}|^2}{2\omega})\to 0$ as $\varepsilon\to 0$ on this support. Together with Parseval's theorem, this can be used to complete the proof. ∎

Another way to write the formulas in Theorem 3.1 for $p^{\mathrm{D}}_{\mathrm{T}}$ and $p^{\mathrm{D}}_{\mathrm{R}}$ is

$$\check{p}^{\mathrm{D}}_{\mathrm{T}}(\omega,\boldsymbol{x}) = -\frac{\mathcal{T}_0}{4\pi}\int\check{\mathcal{T}}(\omega,-L,0,\boldsymbol{x},\boldsymbol{x}')\check{\chi}(\omega,\boldsymbol{x}')d\boldsymbol{x}',$$
$$\check{p}^{\mathrm{D}}_{\mathrm{R}}(\omega,\boldsymbol{x}) = -\frac{\mathcal{R}_0}{4\pi}\int\check{\mathcal{R}}(\omega,-L,0,\boldsymbol{x},\boldsymbol{x}')\check{\chi}(\omega,\boldsymbol{x}')d\boldsymbol{x}',$$

where the kernels of the operators $\check{\mathcal{R}}$ and $\check{\mathcal{T}}$ solve the equations

$$\frac{\partial}{\partial z}\check{\mathcal{R}}(\omega,-L,z,\boldsymbol{x},\boldsymbol{x}') = \frac{i}{2\omega}(\Delta_{\boldsymbol{x}}+\Delta_{\boldsymbol{x}'})\check{\mathcal{R}}(\omega,-L,z,\boldsymbol{x},\boldsymbol{x}'),$$
$$\frac{\partial}{\partial z}\check{\mathcal{T}}(\omega,-L,z,\boldsymbol{x},\boldsymbol{x}') = \frac{i}{2\omega}\Delta_{\boldsymbol{x}'}\check{\mathcal{T}}(\omega,-L,z,\boldsymbol{x},\boldsymbol{x}'),$$

subject to the condition that they are the kernels of the identity at $z=-L$. These should be compared with the diffusion models appearing in Proposition 4.1. In this representation the reflection operator is random due to the driving Brownian terms; this captures in a distributional sense the random character that the reflection operator takes on due to the presence of the microscale fluctuations. What we see is that the random fluctuations precisely add the Brownian terms.

We now take a slightly different perspective and look at how well the solutions of (3.1) on $-L<z<0$ can be approximated by solutions of a decoupled system of paraxial equations. To accomplish this we replace each of the factors in (3.3) by an approximation. First, as we shall soon see, it is in fact sufficient to use the zero-order expansions of $\mathcal{Q}$ and $\mathcal{Q}^{-1}$ about $|\boldsymbol{\kappa}|^2/\omega^2=0$, which are given by

$$\widetilde{\mathcal{Q}}(\omega) = \begin{pmatrix}\sqrt{\frac{1}{\omega}} & \sqrt{\frac{1}{\omega}}\\ i\sqrt{\omega} & -i\sqrt{\omega}\end{pmatrix}\quad\text{and}\quad \widetilde{\mathcal{Q}}^{-1}(\omega) = \frac{1}{2}\begin{pmatrix}\sqrt{\omega} & -i\sqrt{\frac{1}{\omega}}\\ \sqrt{\omega} & i\sqrt{\frac{1}{\omega}}\end{pmatrix}.$$

We may also replace λ by a second-order expansion, giving the following approximate solution of (3.1) on $\{-L < z < 0\}$ with $p^{\mathrm{A}}(t, 0^-, \boldsymbol{x}) = \varphi_p(t, \boldsymbol{x})$ and $v^{\mathrm{A}}(t, 0^-, \boldsymbol{x}) = \varphi_v(t, \boldsymbol{x})$:

$$\begin{pmatrix} p^{\mathrm{A}}(\cdot, z, \cdot) \\ v^{\mathrm{A}}(\cdot, z, \cdot) \end{pmatrix} = \mathcal{P}^{\mathrm{A}}(z) \begin{pmatrix} \varphi_p \\ \varphi_v \end{pmatrix}, \tag{3.8}$$

where the approximate propagator is defined by

$$\mathcal{P}^{\mathrm{A}}(z) \begin{pmatrix} \varphi_p \\ \varphi_v \end{pmatrix} := \widetilde{\mathcal{Q}}(D_t) \begin{pmatrix} e^{\,i\,z\,D_t\left(1-\frac{|D_{\boldsymbol{x}}|^2}{2D_t^2}\right)} & 0 \\ 0 & e^{-i\,z\,D_t\left(1-\frac{|D_{\boldsymbol{x}}|^2}{2D_t^2}\right)} \end{pmatrix} \widetilde{\mathcal{Q}}^{-1}(D_t) \begin{pmatrix} \varphi_p \\ \varphi_v \end{pmatrix}. \tag{3.9}$$

We now have the following result for how well $(p^{\mathrm{A}}, v^{\mathrm{A}})$, given in terms of the operator $\mathcal{P}^{\mathrm{A}}(z)$, approximates the actual solution $(p^{\mathrm{D}}, v^{\mathrm{D}})$, given in terms of $\mathcal{P}^{\mathrm{D}}(z)$.

THEOREM 3.2. *Suppose that $\widehat{\varphi_p}$ and $\widehat{\varphi_v}$ have compact support contained in the set $\{2\omega - |\boldsymbol{\kappa}|^2 > 0\} \cap \{\omega > 1/\varepsilon^4\}$ for a given $\varepsilon < 1/\sqrt{2}$. Then for $-L < z < 0$ there is a constant C depending only on L such that*

$$\left\| \pi_p \circ \left(\mathcal{P}^{\mathrm{D}}(z) - \mathcal{P}^{\mathrm{A}}(z) \right) \begin{pmatrix} \varphi_p \\ \varphi_v \end{pmatrix} \right\|_{L^2} \leq C \left(\varepsilon^4 \left\| \varphi_p \right\|_{L^2} + \varepsilon^8 \left\| \varphi_v \right\|_{L^2} \right)$$

and

$$\left\| \pi_v \circ \left(\mathcal{P}^{\mathrm{D}}(z) - \mathcal{P}^{\mathrm{A}}(z) \right) \begin{pmatrix} \varphi_p \\ \varphi_v \end{pmatrix} \right\|_{L^2} \leq C \left(\left\| \varphi_p \right\|_{L^2} + \varepsilon^4 \left\| \varphi_v \right\|_{L^2} \right),$$

where π_p and π_v are the projections respectively onto the first and second components (that is, the "p" and "v" components) and L^2 means $L^2(\mathbb{R}_t \times \mathbb{R}^d_{\boldsymbol{x}}, \mathbb{R})$. Here, the $\circ$ denotes composition of operators.

Remark 3.3. The difference between the two estimates in the theorem reflects the fact that v should in general have one degree less regularity than p.

Proof. On the support of $\widehat{\varphi_p}$ and $\widehat{\varphi_v}$ we can bound the differences $e^{\pm i\lambda} - e^{\pm i\omega(1-\frac{|\boldsymbol{\kappa}|^2}{2\omega^2})}$ and $\lambda^{1/2} - \sqrt{\omega}$ in terms of ε. Doing so and applying Parseval's theorem gives the estimates. ∎

Additionally we can introduce a directional decomposition of the approximate solution

$$\begin{pmatrix} a^{\mathrm{A}}(\cdot, z, \cdot) \\ b^{\mathrm{A}}(\cdot, z, \cdot) \end{pmatrix} = \begin{pmatrix} e^{-i\,z\,D_t} & 0 \\ 0 & e^{i\,z\,D_t} \end{pmatrix} \widetilde{\mathcal{Q}}^{-1}(D_t)\, \mathcal{P}^{\mathrm{A}}(z) \begin{pmatrix} \varphi_p \\ \varphi_v \end{pmatrix}. \tag{3.10}$$

It is easy to check that this decomposition satisfies the decoupled equations

$$\frac{\partial \check{a}^{\mathrm{A}}}{\partial z} = \frac{i}{2\omega} \Delta_{\boldsymbol{x}} \check{a}^{\mathrm{A}},$$
$$\frac{\partial \check{b}^{\mathrm{A}}}{\partial z} = -\frac{i}{2\omega} \Delta_{\boldsymbol{x}} \check{b}^{\mathrm{A}}.$$

Thus by Theorem 3.2 we can approximate solutions p of the original equation (2.1) up to accuracy $\approx \varepsilon^4$ by solving these decoupled paraxial equations.

3.2. Riccati equations. We use the decomposition (3.10) for the approximate solution, also in the presence of random fluctuations. Indeed, if p and v denote our solution of (2.1) with the fluctuations, then

$$\begin{pmatrix} a \\ b \end{pmatrix}(t,z,\boldsymbol{x}) := \begin{pmatrix} e^{-i\,z\,D_t} & 0 \\ 0 & e^{i\,z\,D_t} \end{pmatrix} \widetilde{\mathcal{Q}}^{-1}(D_t) \begin{pmatrix} p \\ v \end{pmatrix}(t,z,\boldsymbol{x})$$

is our directional decomposition. This is actually only an approximation of the true decomposition given by (3.5). It is also convenient to rescale a and b,

$$a^\varepsilon(t,z,\boldsymbol{x}) = a(\varepsilon^4 t, z, \varepsilon^2 \boldsymbol{x}), \qquad b^\varepsilon(t,z,\boldsymbol{x}) = b(\varepsilon^4 t, z, \varepsilon^2 \boldsymbol{x}),$$

and to work in the frequency domain by considering $\breve{a}^\varepsilon$ and $\breve{b}^\varepsilon$. Using (2.1), we obtain the following exact system for $-L < z < 0$:

$$\frac{\partial \breve{a}^\varepsilon}{\partial z} = \left(\frac{i\omega}{2\varepsilon}\,\nu\left(\frac{z}{\varepsilon^2},\boldsymbol{x}\right) + \frac{i}{2\omega}\Delta_{\boldsymbol{x}}\right)\breve{a}^\varepsilon + e^{-2i\omega\frac{z}{\varepsilon^4}}\left(\frac{i\omega}{2\varepsilon}\,\nu\left(\frac{z}{\varepsilon^2},\boldsymbol{x}\right) + \frac{i}{2\omega}\Delta_{\boldsymbol{x}}\right)\breve{b}^\varepsilon, \tag{3.11}$$

$$\frac{\partial \breve{b}^\varepsilon}{\partial z} = -e^{2i\omega\frac{z}{\varepsilon^4}}\left(\frac{i\omega}{2\varepsilon}\,\nu\left(\frac{z}{\varepsilon^2},\boldsymbol{x}\right) + \frac{i}{2\omega}\Delta_{\boldsymbol{x}}\right)\breve{a}^\varepsilon - \left(\frac{i\omega}{2\varepsilon}\,\nu\left(\frac{z}{\varepsilon^2},\boldsymbol{x}\right) + \frac{i}{2\omega}\Delta_{\boldsymbol{x}}\right)\breve{b}^\varepsilon. \tag{3.12}$$

We approximate the condition that there are no incoming waves by asking that $\breve{a}^\varepsilon(\omega,-L^-,\boldsymbol{x}) = 0$ and $\breve{b}^\varepsilon(\omega,0^+,\boldsymbol{x}) = 0$. This leads to the following boundary and jump conditions:

$$\breve{b}^\varepsilon(\omega,0^-,\boldsymbol{x}) = -\frac{\sqrt{\omega}}{2\varepsilon^2}\,\breve{\chi}(\omega,\boldsymbol{x}), \quad \breve{a}^\varepsilon(\omega,-L^+,\boldsymbol{x}) = \mathcal{R}_0 e^{2i\omega\frac{L}{\varepsilon^4}}\breve{b}^\varepsilon(\omega,-L^+,\boldsymbol{x}),$$

$$\breve{b}^\varepsilon(\omega,-L^-,\boldsymbol{x}) = \mathcal{T}_0\breve{b}^\varepsilon(\omega,-L^+,\boldsymbol{x}), \qquad \breve{a}^\varepsilon(\omega,0^+,\boldsymbol{x}) = \breve{a}^\varepsilon(\omega,0^-,\boldsymbol{x}) + \frac{\sqrt{\omega}}{2\varepsilon^2}\,\breve{\chi}(\omega,\boldsymbol{x}),$$

where $\mathcal{R}_0$ and $\mathcal{T}_0$ are the same as in (3.7). Indeed, in view of Theorem 3.2 with $\nu = 0$, we expect decoupling of (3.11)–(3.12), with solutions accurate up to order ε^4.

To capture the transmission and reflection of the wave field in the presence of fluctuations, we apply an invariant imbedding approach to obtain a representation valid for $-L < z < 0$:

$$\breve{b}^\varepsilon(\omega,-L^-,\boldsymbol{x}) = \mathcal{T}_0 \int \breve{\mathcal{T}}^\varepsilon(\omega,-L,z,\boldsymbol{x},\boldsymbol{x}')\breve{b}^\varepsilon(\omega,z,\boldsymbol{x}')\,d\boldsymbol{x}', \tag{3.13}$$

$$\breve{a}^\varepsilon(\omega,z,\boldsymbol{x}) = \mathcal{R}_0 e^{2i\omega\frac{L}{\varepsilon^4}} \int \breve{\mathcal{R}}^\varepsilon(\omega,-L,z,\boldsymbol{x},\boldsymbol{x}')\breve{b}^\varepsilon(\omega,z,\boldsymbol{x}')\,d\boldsymbol{x}', \tag{3.14}$$

where the operators $\breve{\mathcal{T}}^\varepsilon$ and $\breve{\mathcal{R}}^\varepsilon$, defined through their kernels, satisfy a natural coupled system of operator Riccati equations which follow from the equations satisfied by the local amplitudes. Indeed, using the mode coupling equations (3.11)–(3.12), we

find that

$$\begin{aligned}\frac{\partial}{\partial z}\check{\mathcal{R}}^\varepsilon(\omega,-L,z,\boldsymbol{x},\boldsymbol{x}') &= \mathcal{R}_0^{-1}e^{-\frac{2i\omega}{\varepsilon^4}(z+L)}\delta(\boldsymbol{x}-\boldsymbol{x}')\left(\frac{i\omega}{2\varepsilon}\nu\left(\frac{z}{\varepsilon^2},\boldsymbol{x}'\right)+\frac{i}{2\omega}\Delta_{\boldsymbol{x}'}\right)\\ &+\mathcal{R}_0 e^{\frac{2i\omega}{\varepsilon^4}(z+L)}\int\check{\mathcal{R}}^\varepsilon(\omega,-L,z,\boldsymbol{x},\boldsymbol{x}_1)\\ &\times\left(\frac{i\omega}{2\varepsilon}\nu\left(\frac{z}{\varepsilon},\boldsymbol{x}_1\right)+\frac{i}{2\omega}\Delta_{\boldsymbol{x}_1}\right)\check{\mathcal{R}}^\varepsilon(\omega,-L,z,\boldsymbol{x}_1,\boldsymbol{x}')\,d\boldsymbol{x}_1\\ &+\left(\frac{i\omega}{2\varepsilon}\nu\left(\frac{z}{\varepsilon^2},\boldsymbol{x}\right)+\frac{i}{2\omega}\Delta_{\boldsymbol{x}}\right)\check{\mathcal{R}}^\varepsilon(\omega,-L,z,\boldsymbol{x},\boldsymbol{x}')\\ &+\check{\mathcal{R}}^\varepsilon(\omega,-L,z,\boldsymbol{x},\boldsymbol{x}')\left(\frac{i\omega}{2\varepsilon}\nu\left(\frac{z}{\varepsilon^2},\boldsymbol{x}'\right)+\frac{i}{2\omega}\Delta_{\boldsymbol{x}'}\right),\end{aligned}\tag{3.15}$$

$$\begin{aligned}\frac{\partial}{\partial z}\check{\mathcal{T}}^\varepsilon(\omega,-L,z,\boldsymbol{x},\boldsymbol{x}') &= \check{\mathcal{T}}^\varepsilon(\omega,-L,z,\boldsymbol{x},\boldsymbol{x}')\left(\frac{i\omega}{2\varepsilon}\nu\left(\frac{z}{\varepsilon^2},\boldsymbol{x}'\right)+\frac{i}{2\omega}\Delta_{\boldsymbol{x}'}\right)\\ &+\mathcal{R}_0 e^{\frac{2i\omega}{\varepsilon^4}(z+L)}\int\check{\mathcal{T}}^\varepsilon(\omega,-L,z,\boldsymbol{x},\boldsymbol{x}_1)\\ &\times\left(\frac{i\omega}{2\varepsilon}\nu\left(\frac{z}{\varepsilon},\boldsymbol{x}_1\right)+\frac{i}{2\omega}\Delta_{\boldsymbol{x}_1}\right)\check{\mathcal{R}}^\varepsilon(\omega,-L,z,\boldsymbol{x}_1,\boldsymbol{x}')\,d\boldsymbol{x}_1.\end{aligned}\tag{3.16}$$

This system is supplemented with the following initial conditions at $z=-L$:

$$\check{\mathcal{R}}^\varepsilon(\omega,-L,z=-L,\boldsymbol{x},\boldsymbol{x}')=\delta(\boldsymbol{x}-\boldsymbol{x}'),\qquad \check{\mathcal{T}}^\varepsilon(\omega,-L,z=-L,\boldsymbol{x},\boldsymbol{x}')=\delta(\boldsymbol{x}-\boldsymbol{x}').$$

In the system (3.15)–(3.16) the first two parameters $-L$ and ω of $\check{\mathcal{R}}^\varepsilon$ and $\check{\mathcal{T}}^\varepsilon$ are frozen. Therefore the systems for different frequencies ω are not related from the analytic point of view, but they are not independent from the statistical point of view since the systems are written in terms of the same realization of the process ν. It turns out that the correlation properties of the reflection and transmission operators play a crucial role in the asymptotic regime $\varepsilon\to 0$, as we will see below.

The transmission and reflection operators evaluated at $z=0$ carry all the relevant information about the random medium from the point of view of the transmitted wave $p^\varepsilon(t,-L^-,\boldsymbol{x}):=p(\varepsilon^4 t,-L^-,\varepsilon^2\boldsymbol{x})$ and the reflected wave $p^\varepsilon(t,0^+,\boldsymbol{x}):=p(\varepsilon^4 t,0^+,\varepsilon^2\boldsymbol{x})$, which are our main quantities of interest. In the frequency domain they can be expressed as

$$\check{p}^\varepsilon(\omega,0^+,\boldsymbol{x})=\frac{\varepsilon^2}{\sqrt{\omega}}\Big\{e^{i\omega\frac{2L}{\varepsilon^4}}\mathcal{R}_0\int\check{\mathcal{R}}^\varepsilon(\omega,-L,0,\boldsymbol{x},\boldsymbol{x}')\check{b}^\varepsilon(\omega,0^-,\boldsymbol{x}')d\boldsymbol{x}'-\check{b}^\varepsilon(\omega,0^-,\boldsymbol{x})\Big\},\tag{3.17}$$

$$\check{p}^\varepsilon(\omega,-L^-,\boldsymbol{x})=\frac{\varepsilon^2}{\sqrt{\omega}}e^{i\omega\frac{L}{\varepsilon^4}}\mathcal{T}_0\int\check{\mathcal{T}}^\varepsilon(\omega,-L,0,\boldsymbol{x}',\boldsymbol{x}')\check{b}^\varepsilon(\omega,0^-,\boldsymbol{x}')d\boldsymbol{x}',\tag{3.18}$$

with $\check{b}^\varepsilon(\omega,0^-,\boldsymbol{x})=-\frac{\sqrt{\omega}}{2\varepsilon^2}\check{\chi}(\omega,\boldsymbol{x})$. We will also need the following representation formula for the field $p^\varepsilon(t,-L_1,\boldsymbol{x}):=p(\varepsilon^4 t,-L_1,\varepsilon^2\boldsymbol{x})$ inside the heterogeneous region:

for $-L < -L_1 < 0$ we have

(3.19)

$$\begin{aligned}&\check{p}^\varepsilon(\omega,-L_1,\boldsymbol{x})\\&=\frac{\varepsilon^2}{\sqrt{\omega}}\Big\{e^{i\omega\frac{2L-L_1}{\varepsilon^4}}\mathcal{R}_0\iint\check{\mathcal{R}}^\varepsilon(\omega,-L,-L_1,\boldsymbol{x},\boldsymbol{x}'')\check{\mathcal{T}}^\varepsilon(\omega,-L_1,0,\boldsymbol{x}'',\boldsymbol{x}')d\boldsymbol{x}''\check{b}^\varepsilon(\omega,0^-,\boldsymbol{x}')d\boldsymbol{x}'\\&\qquad+e^{i\omega\frac{L_1}{\varepsilon^4}}\int\check{\mathcal{T}}^\varepsilon(\omega,-L_1,0,\boldsymbol{x}',\boldsymbol{x}')\check{b}^\varepsilon(\omega,0^-,\boldsymbol{x}')d\boldsymbol{x}'\Big\}.\end{aligned}$$

In the scaling regime $\varepsilon\to 0$ we are able to deduce from the system (3.15)–(3.16) a description in terms of effective white noise models for the transmission and reflection operators, at least on the level of moments. We describe this in the next section.

4. Itô–Schrödinger diffusion models for transmitted and reflected fields. We center according to the travel time associated with the deterministic medium component and define the transmitted and reflected pressure fields by

$$p^\varepsilon_{\mathrm{R}}(s,\boldsymbol{x}):=p(2L+\varepsilon^4 s,0^+,\varepsilon^2\boldsymbol{x})-\frac{1}{2}\chi(2L/\varepsilon^4+s,\boldsymbol{x}),\tag{4.1}$$

$$p^\varepsilon_{\mathrm{T}}(s,\boldsymbol{x}):=p(L+\varepsilon^4 s,-L^-,\varepsilon^2\boldsymbol{x}).\tag{4.2}$$

The field $p^\varepsilon_{\mathrm{T}}(s,\boldsymbol{x})$ is the field observed just below the bottom interface at $z=-L^-$ around the expected arrival time L; the field $p^\varepsilon_{\mathrm{R}}(s,\boldsymbol{x})$ is the field observed just above the top interface at $z=0^+$ coming from the reflection off the boundary at $z=-L$, and observed around the expected arrival time $2L$. Using (3.17)–(3.18), these can be written as

$$p^\varepsilon_{\mathrm{R}}(s,\boldsymbol{x})=-\frac{\mathcal{R}_0}{4\pi}\iint\check{\mathcal{R}}^\varepsilon(\omega,-L,0,\boldsymbol{x},\boldsymbol{x}')\,\check{\chi}(\omega,\boldsymbol{x}')\,d\boldsymbol{x}'e^{-i\omega s}\,d\omega,\tag{4.3}$$

$$p^\varepsilon_{\mathrm{T}}(s,\boldsymbol{x})=-\frac{\mathcal{T}_0}{4\pi}\iint\check{\mathcal{T}}^\varepsilon(\omega,-L,0,\boldsymbol{x},\boldsymbol{x}')\,\check{\chi}(\omega,\boldsymbol{x}')\,d\boldsymbol{x}'e^{-i\omega s}\,d\omega.\tag{4.4}$$

These fields are now characterized via effective scaling limit models for the transmission and reflection operators, as follows.

PROPOSITION 4.1. *The processes $(p^\varepsilon_{\mathrm{T}}(s,\boldsymbol{x}))_{s\in\mathbb{R},\boldsymbol{x}\in\mathbb{R}^d}$, $(p^\varepsilon_{\mathrm{R}}(s,\boldsymbol{x}))_{s\in\mathbb{R},\boldsymbol{x}\in\mathbb{R}^d}$ converge in distribution as $\varepsilon\to 0$ in the space $C^0(\mathbb{R},L^2(\mathbb{R}^d,\mathbb{R}))\cap L^2(\mathbb{R},L^2(\mathbb{R}^d,\mathbb{R}))$ to the limit process $(p_{\mathrm{T}}(s,\boldsymbol{x}))_{s\in\mathbb{R},\boldsymbol{x}\in\mathbb{R}^d}$, $(p_{\mathrm{R}}(s,\boldsymbol{x}))_{s\in\mathbb{R},\boldsymbol{x}\in\mathbb{R}^d}$ given by*

$$p_{\mathrm{R}}(s,\boldsymbol{x})=-\frac{\mathcal{R}_0}{4\pi}\iint\check{\mathcal{R}}(\omega,-L,0,\boldsymbol{x},\boldsymbol{x}')\,\check{\chi}(\omega,\boldsymbol{x}')\,d\boldsymbol{x}'e^{-i\omega s}\,d\omega,\tag{4.5}$$

$$p_{\mathrm{T}}(s,\boldsymbol{x})=-\frac{\mathcal{T}_0}{4\pi}\iint\check{\mathcal{T}}(\omega,-L,0,\boldsymbol{x},\boldsymbol{x}')\,\check{\chi}(\omega,\boldsymbol{x}')\,d\boldsymbol{x}'e^{-i\omega s}\,d\omega,\tag{4.6}$$

where the variables $\mathcal{T}_0$ and $\mathcal{R}_0$ are defined by (3.7). *The kernels of the operators $(\check{\mathcal{R}}(\omega,-L,z,\boldsymbol{x},\boldsymbol{x}'))_{z\in[-L,0]}$ and $(\check{\mathcal{T}}(\omega,-L,z,\boldsymbol{x},\boldsymbol{x}'))_{z\in[-L,0]}$ are the solutions of the following Itô–Schrödinger diffusion models:*

$$\begin{aligned}d\check{\mathcal{R}}(\omega,-L,z,\boldsymbol{x},\boldsymbol{x}')&=\frac{i}{2\omega}\left(\Delta_{\boldsymbol{x}}+\Delta_{\boldsymbol{x}'}\right)\check{\mathcal{R}}(\omega,-L,z,\boldsymbol{x},\boldsymbol{x}')\,dz\\&\quad+\frac{i\omega}{2}\check{\mathcal{R}}(\omega,-L,z,\boldsymbol{x},\boldsymbol{x}')\circ\left(dB(z,\boldsymbol{x})+dB(z,\boldsymbol{x}')\right),\end{aligned}\tag{4.7}$$

$$\begin{aligned}d\check{\mathcal{T}}(\omega,-L,z,\boldsymbol{x},\boldsymbol{x}')&=\frac{i}{2\omega}\Delta_{\boldsymbol{x}'}\check{\mathcal{T}}(\omega,-L,z,\boldsymbol{x},\boldsymbol{x}')\,dz\\&\quad+\frac{i\omega}{2}\check{\mathcal{T}}(\omega,-L,z,\boldsymbol{x},\boldsymbol{x}')\circ dB(z,\boldsymbol{x}'),\end{aligned}\tag{4.8}$$

with the initial conditions at $z=-L$ being

$$\check{\mathcal{R}}(\omega,-L,z=-L,\boldsymbol{x},\boldsymbol{x}')=\delta(\boldsymbol{x}-\boldsymbol{x}'),\qquad \check{\mathcal{T}}(\omega,-L,z=-L,\boldsymbol{x},\boldsymbol{x}')=\delta(\boldsymbol{x}-\boldsymbol{x}').$$

The symbol $\circ$ stands for the Stratonovich stochastic integral [8]*, and $B(z,\boldsymbol{x})$ is a real-valued Brownian field with covariance*

$$\mathbb{E}[B(z_1,\boldsymbol{x}_1)B(z_2,\boldsymbol{x}_2)]=\min\{z_1,z_2\}D(\boldsymbol{x}_1-\boldsymbol{x}_2). \tag{4.9}$$

Making use of (3.19) and of the semigroup property [8] of the effective operators, we also find that the joint law for the direct arrival at the two points of observation located at $(-L_1,\varepsilon^2\boldsymbol{x}_1)$ and $(-L_2,\varepsilon^2\boldsymbol{x}_2)$, with $-L\le -L_2\le -L_1\le 0$, can be characterized by

(4.10)

$$p(L_1+\varepsilon^4 s,-L_1,\varepsilon^2\boldsymbol{x}_1)\simeq -\frac{1}{4\pi}\iint \check{\mathcal{T}}(\omega,-L_1,0,\boldsymbol{x}_1,\boldsymbol{y}_1)\,\check{\chi}(\omega,\boldsymbol{y}_1)\,d\boldsymbol{y}_1 e^{-i\omega s}d\omega,$$

$$\begin{aligned} p(L_2+\varepsilon^4 s,-L_2,\varepsilon^2\boldsymbol{x}_2)\simeq -\frac{1}{4\pi}\int\iint \check{\mathcal{T}}(\omega,-L_2,-L_1,\boldsymbol{x}_2,\boldsymbol{y}_2)\check{\mathcal{T}}(\omega,-L_1,0,\boldsymbol{y}_2,\boldsymbol{y}_1)\\ \times\check{\chi}(\omega,\boldsymbol{y}_1)\,d\boldsymbol{y}_1 d\boldsymbol{y}_2 e^{-i\omega s}d\omega. \end{aligned} \tag{4.11}$$

The independence of the increments of the Brownian field implies that, for $-L\le -L_2\le -L_1\le 0$, the operators $\check{\mathcal{T}}(\omega,-L,-L_2,\boldsymbol{x},\boldsymbol{x}')$ and $\check{\mathcal{R}}(\omega,-L,-L_2,\boldsymbol{x},\boldsymbol{x}')$ are statistically independent of $\check{\mathcal{T}}(\omega,-L_2,-L_1,\boldsymbol{x},\boldsymbol{x}')$ and $\check{\mathcal{R}}(\omega,-L_2,-L_1,\boldsymbol{x},\boldsymbol{x}')$, which we exploit in evaluating the cross correlation. We remark here also that the transmission operator over the subslab $(-L_1,0)$ appears in both expressions in (4.10)–(4.11), and it is this pairing that will lead to an expression for the cross correlation in terms of a statistically stable filter or transformation below. The general statistical properties of the operators $\check{\mathcal{R}},\check{\mathcal{T}}$ were studied in [11].

We consider next the other main contributions to the field observations at $(-L_1,\varepsilon^2\boldsymbol{x}_1)$ and $(-L_2,\varepsilon^2\boldsymbol{x}_2)$, namely the ones associated with the wave propagating from the surface to the interface at $z=-L$ and back to the observation points. Again, making use of the semigroup property of the effective operators, we find that the joint law for these "secondary" arrivals at the two points of observation located at $(-L_1,\varepsilon^2\boldsymbol{x}_1)$ and $(-L_2,\varepsilon^2\boldsymbol{x}_2)$, with $-L\le -L_2\le -L_1\le 0$, can in our scaling regime be characterized by

$$\begin{aligned} &p(2L-L_1+\varepsilon^4 s,-L_1,\varepsilon^2\boldsymbol{x}_1)\\ &\simeq -\frac{\mathcal{R}_0}{4\pi}\int\iiint \check{\mathcal{T}}(\omega,-L_1,-L_2,\boldsymbol{x}_1,\boldsymbol{y}_3)\check{\mathcal{R}}(\omega,-L,-L_2,\boldsymbol{y}_3,\boldsymbol{y}_2)\\ &\quad\times\check{\mathcal{T}}(\omega,-L_2,0,\boldsymbol{y}_2,\boldsymbol{y}_1)\check{\chi}(\omega,\boldsymbol{y}_1)\,d\boldsymbol{y}_1\,d\boldsymbol{y}_2\,d\boldsymbol{y}_3 e^{-i\omega s}d\omega, \end{aligned} \tag{4.12}$$

$$\begin{aligned} &p(2L-L_2+\varepsilon^4 s,-L_2,\varepsilon^2\boldsymbol{x}_2)\\ &\simeq -\frac{\mathcal{R}_0}{4\pi}\int\iint \check{\mathcal{R}}(\omega,-L,-L_2,\boldsymbol{x}_2,\boldsymbol{y}_2)\check{\mathcal{T}}(\omega,-L_2,0,\boldsymbol{y}_2,\boldsymbol{y}_1)\\ &\quad\times\check{\chi}(\omega,\boldsymbol{y}_1)\,d\boldsymbol{y}_1 d\boldsymbol{y}_2 e^{-i\omega s}d\omega. \end{aligned} \tag{4.13}$$

We used the particular representation above to show how the transmission operator over the subslab $(-L_2,0)$ appears in both expressions in (4.12)–(4.13) and correspondingly for the reflection operator over the subslab $(-L,-L_2)$. Such a pairing will lead to an expression for the corresponding cross correlation in terms of a statistically stable filter, as we discuss below.

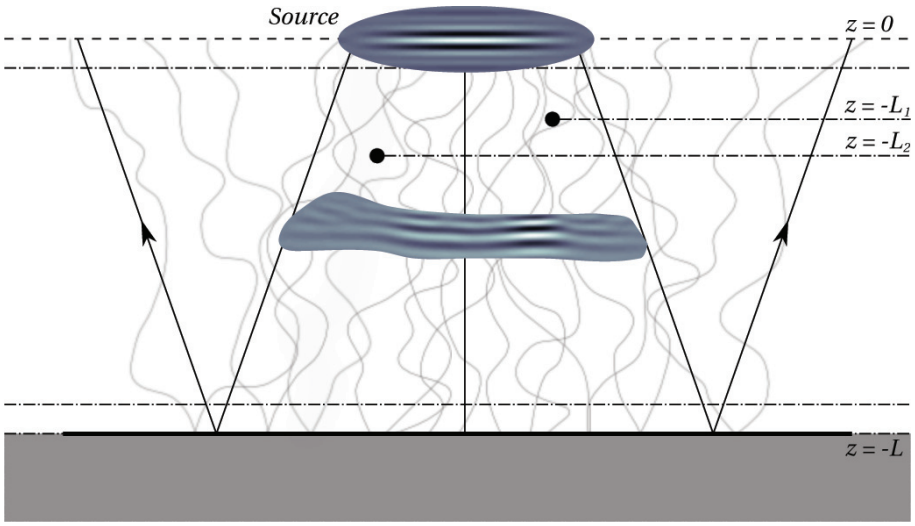

FIG. 5.1. *Configuration. The source is located at the surface $z = 0$. An interface is present at depth $-L$. We compute the correlation between the two points at depths $-L_1$ and $-L_2$. The random fluctuations occur in the region $z \in (-L, 0)$.*

5. Characterization of cross correlations. Here, we characterize the "field-field" cross correlation function between the points $(-L_1, \varepsilon^2 \boldsymbol{x}_1)$ and $(-L_2, \varepsilon^2 \boldsymbol{x}_2)$. We assume that $T \gg L$ and $0 < L_1 < L_2 < L$. The field-field correlation function is given by

$$\mathcal{V}_T^\varepsilon(t) = \int_0^T p(t', -L_1, \varepsilon^2 \boldsymbol{x}_1) p(t' + t, -L_2, \varepsilon^2 \boldsymbol{x}_2)\, dt'. \tag{5.1}$$

Note that the source function χ and the pressure field are real-valued. The configuration is illustrated in Figure 5.1; we compute the correlation between the two points at depths $-L_1$ and $-L_2$.

In Figures 5.2 and 5.3 respectively we show an example of a random velocity field and how a wave packet propagating through this is affected relative to the homogeneous case.

We will see that the wave field correlation function concentrates around specific time lags t that correspond to travel times between the two observation points, and that the time extent of the correlation function around these time lags is of order ε^4, i.e., of the same order as the source pulse width.

Under the scaling assumptions of section 2 we find that the correlations in (5.1) have leading contributions centered at four particular time lags:

$$\mathcal{V}_T^\varepsilon\big(\pm(L_2 - L_1) + \varepsilon^4 s\big)/\varepsilon^4 \simeq \mathcal{V}_{\mathrm{t}}^{\pm}(s)\,, \tag{5.2}$$

$$\mathcal{V}_T^\varepsilon\big(\pm(2L - L_1 - L_2) + \varepsilon^4 s\big)/\varepsilon^4 \simeq \mathcal{V}_{\mathrm{r}}^{\pm}(s)\,. \tag{5.3}$$

Here, the amplitude scaling corresponds to a rescaling of the source time traces so that they have order one energy, but it plays no significant role as the problem is linear. The contribution $\mathcal{V}_{\mathrm{t}}^{+}$ (resp., $\mathcal{V}_{\mathrm{t}}^{-}$) corresponds to the correlation of wave components directly transmitted between the points of observation of transmitted (resp., reflected) waves. More exactly, the contribution $\mathcal{V}_{\mathrm{t}}^{+}$ (around time lag $+(L_2 - L_1)$) comes from

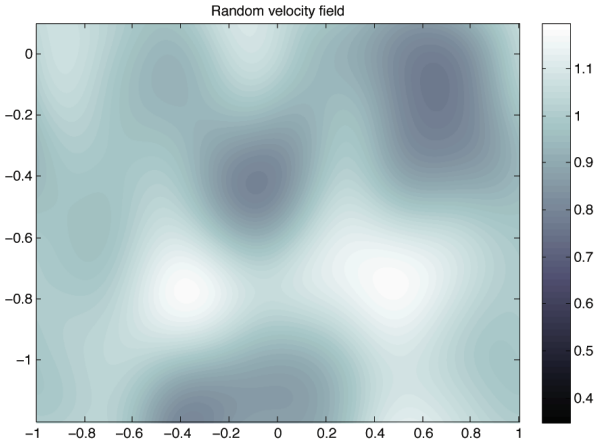

FIG. 5.2. *A realization of a random velocity field. The random velocity fluctuations constitute a (truncated) homogeneous Gaussian random field with a Gaussian correlation function simulated using the FFT. The correlation length of the random medium is* 0.22*, and the standard deviation of the fluctuations is* 0.097*.*

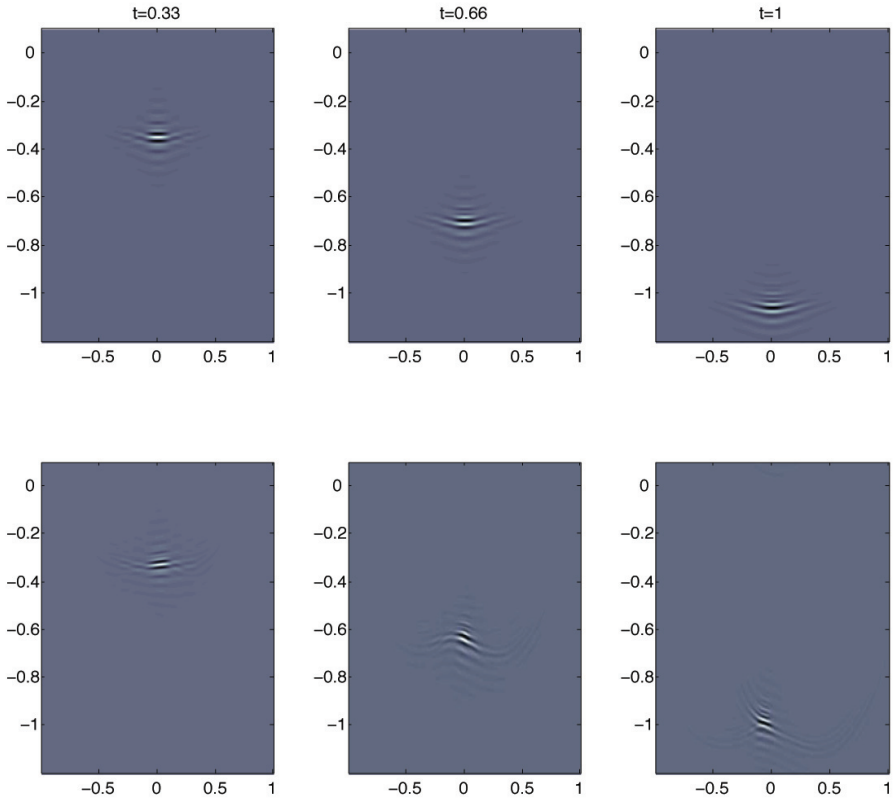

FIG. 5.3. *The wave packet propagating in a homogeneous medium (top row) or in a random medium (bottom row) at the same three times, for the velocity field in Figure* 5.2*. It is evident that the random medium fluctuations on the scale of the lateral source support deform the wavefront. Here the wavelength is* 0.046*, the background speed is* 0.99*, and the lateral source support* $R_0 = 0.21$*.*

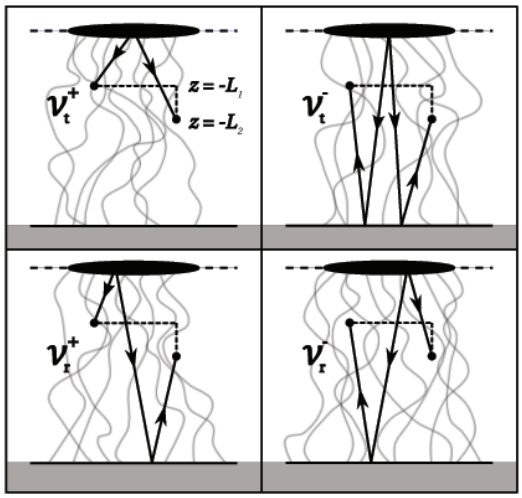

FIG. 5.4. *The four contributions to the cross correlation between points* $(-L_1, \varepsilon^2 \boldsymbol{x}_1)$ *and* $(-L_2, \varepsilon^2 \boldsymbol{x}_2)$.

the correlation between the waves that propagate from the surface to the depth $-L_1$ and then to the depth $-L_2$ (see Figure 5.4, top left). The contribution $\mathcal{V}_{\mathrm{t}}^{-}$ (around time lag $-(L_2 - L_1)$) comes from the correlation between the waves that have been reflected by the interface at $z = -L$ and that propagate from this interface to the depth $-L_2$ and then to the depth $-L_1$ (Figure 5.4, top right). We stress here that these wave components have been strongly affected by the multiple scattering in the medium, and understanding how this affects the relation of the components $\mathcal{V}$ and the Green's functions is our main objective. The contributions $\mathcal{V}_{\mathrm{r}}^{+}$ and $\mathcal{V}_{\mathrm{r}}^{-}$ correspond to crossed terms. The contribution $\mathcal{V}_{\mathrm{r}}^{+}$ (around time lag $2L - L_1 - L_2$) comes from correlation between the waves that have propagated from the surface to the reflector at depth $-L$ and then back to the depth $-L_2$ with the waves that have traveled directly to depth $-L_1$ (Figure 5.4, bottom left). The contribution $\mathcal{V}_{\mathrm{r}}^{-}$ (around time lag $-(2L - L_1 - L_2)$) comes from correlation between the waves that have propagated from the surface to the reflector at depth $-L$ and then back to the depth $-L_1$ with the waves that has traveled directly to depth $-L_2$ (Figure 5.4, bottom right). We remark here that the two last terms $\mathcal{V}_{\mathrm{r}}^{\pm}$ give contributions for larger time lags than the first two contributions $\mathcal{V}_{\mathrm{t}}^{\pm}$ (since $2L - L_1 - L_2 > L_2 - L_1$) and could be used for estimation of the depth of the bottom interface.

6. Integral expressions for correlation components. The correlation component $\mathcal{V}_{\mathrm{t}}^{+}$ can be characterized in distribution in the scaling limit $\varepsilon \to 0$ by the following expression using (4.10), (4.11), and the definition (5.1):

$$\mathcal{V}_{\mathrm{t}}^{+}(s) = \frac{1}{2\pi} \iint \check{\Lambda}_{\mathrm{t}}^{+}(\omega, \boldsymbol{x}; \boldsymbol{x}_1, L_1) \check{\mathcal{T}}(\omega, -L_2, -L_1, \boldsymbol{x}_2, \boldsymbol{x}_1 - \boldsymbol{x}) d\boldsymbol{x} e^{-i\omega s} d\omega, \tag{6.1}$$

where $\check{\mathcal{T}}(\omega, -L, z, \boldsymbol{x}, \boldsymbol{x}')$ is defined by (4.8). Remember that $\check{\mathcal{T}}(\omega, -L_2, -L_1, \boldsymbol{x}_2, \boldsymbol{x}_1)$ is the (rescaled) paraxial Green's function from the point $(-L_1, \varepsilon^2 \boldsymbol{x}_1)$ to the point $(-L_2, \varepsilon^2 \boldsymbol{x}_2)$. Therefore, (6.1) reads as a filtered version of the causal Green's function between the two points of observation. Indeed we assume the paraxial scaling and consider the Green's function or transmission operator associated with this regime;

thus only consecutive observation points located in the forward cone of wave energy give a significant contribution. We discuss the shape of the filter in more detail in section 9.

The filter is

$$\check{\Lambda}_{\mathrm{t}}^{+}(\omega,\boldsymbol{x};\boldsymbol{x}_1,L_1) = \frac{1}{4}\iint \check{\mathcal{T}}(\omega,-L_1,0,\boldsymbol{x}_1-\boldsymbol{x},\boldsymbol{y}_2)\overline{\check{\mathcal{T}}(\omega,-L_1,0,\boldsymbol{x}_1,\boldsymbol{y}_1)}\check{\chi}(\omega,\boldsymbol{y}_2)\overline{\check{\chi}(\omega,\boldsymbol{y}_1)}d\boldsymbol{y}_1 d\boldsymbol{y}_2. \tag{6.2}$$

In the strongly cluttered scaling regime described in section 8 the filter $\check{\Lambda}_{\mathrm{t}}^{+}$ is self-averaging in the sense that it is approximately equal to its expectation [4]:

$$\mathbb{E}[\check{\Lambda}_{\mathrm{t}}^{+}(\omega,\boldsymbol{x};\boldsymbol{x}_1,L_1)] = \frac{1}{4}\iint \mathbb{E}\big[\check{\mathcal{T}}(\omega,-L_1,0,\boldsymbol{x}_1-\boldsymbol{x},\boldsymbol{y}_2)\overline{\check{\mathcal{T}}(\omega,-L_1,0,\boldsymbol{x}_1,\boldsymbol{y}_1)}\big] \times \check{\chi}(\omega,\boldsymbol{y}_2)\overline{\check{\chi}(\omega,\boldsymbol{y}_1)}d\boldsymbol{y}_1 d\boldsymbol{y}_2\,. \tag{6.3}$$

Note that the fact that the filter is statistically stable is important from the theoretical point of view, as it allows us to perform a detailed resolution analysis. It is important in practice because it guarantees that the quality of the Green's function estimation does not depend on the particular realization of the medium. It can also be used in order to improve the quality of the estimation: if the statistical distribution of the random medium is known, then the properties of the filter can be fully characterized (as is done in the next section) so that it is possible to (partially) deconvolve the effect of the filter and to enhance the estimation of the Green's function.

Similarly we have, using the representations (4.12), (4.13),

$$\mathcal{V}_{\mathrm{t}}^{-}(s) = \frac{\mathcal{R}_0^2}{2\pi}\iint \check{\Lambda}_{\mathrm{t}}^{-}(\omega,\boldsymbol{x};\boldsymbol{x}_2,L_2,L)\check{\mathcal{T}}(\omega,-L_1,-L_2,\boldsymbol{x}_1,\boldsymbol{x}_2-\boldsymbol{x})d\boldsymbol{x}e^{-i\omega s}d\omega, \tag{6.4}$$

with the filter

$$\check{\Lambda}_{\mathrm{t}}^{-}(\omega,\boldsymbol{x};\boldsymbol{x}_2,L_2,L) = \frac{1}{4}\iint \check{\mathcal{T}}(\omega,-L_2,0,\boldsymbol{y}_4,\boldsymbol{y}_2)\overline{\check{\mathcal{T}}(\omega,-L_2,0,\boldsymbol{y}_3,\boldsymbol{y}_1)} \times \check{\mathcal{R}}(\omega,-L,-L_2,\boldsymbol{x}_2-\boldsymbol{x},\boldsymbol{y}_4)\overline{\check{\mathcal{R}}(\omega,-L,-L_2,\boldsymbol{x}_2,\boldsymbol{y}_3)}\check{\chi}(\omega,\boldsymbol{y}_2)\overline{\check{\chi}(\omega,\boldsymbol{y}_1)}d\boldsymbol{y}_1 d\boldsymbol{y}_2 d\boldsymbol{y}_3 d\boldsymbol{y}_4\,.$$

Using reciprocity and the fact that $\mathcal{V}_{\mathrm{t}}^{-}(s)$ is real-valued, we have

$$\mathcal{V}_{\mathrm{t}}^{-}(s) = \frac{\mathcal{R}_0^2}{2\pi}\iint \overline{\check{\Lambda}_{\mathrm{t}}^{-}(\omega,\boldsymbol{x};\boldsymbol{x}_2,L_2,L)}\check{\mathcal{T}}(\omega,-L_2,-L_1,\boldsymbol{x}_2-\boldsymbol{x},\boldsymbol{x}_1)d\boldsymbol{x}e^{i\omega s}d\omega, \tag{6.5}$$

which shows that we obtain a filtered version of the anticausal Green's function between the two points of observation (note the sign in the exponent $e^{i\omega s}$). Again, in the strongly cluttered scaling regime described in section 8, the filter $\check{\Lambda}_{\mathrm{t}}^{-}$ is self-averaging in the sense that it is approximately equal to its expectation. Moreover, the independence of the kernels $\check{\mathcal{T}}(\omega,-L_2,0,\cdot,\cdot)$ and $\check{\mathcal{R}}(\omega,-L,-L_2,\cdot,\cdot)$ implies that

$$\mathbb{E}[\check{\Lambda}_{\mathrm{t}}^{-}(\omega,\boldsymbol{x};\boldsymbol{x}_2,L_2,L)] = \frac{1}{4}\iint \mathbb{E}\Big[\check{\mathcal{T}}(\omega,-L_2,0,\boldsymbol{y}_4,\boldsymbol{y}_2)\overline{\check{\mathcal{T}}(\omega,-L_2,0,\boldsymbol{y}_3,\boldsymbol{y}_1)}\Big] \times \mathbb{E}\Big[\check{\mathcal{R}}(\omega,-L,-L_2,\boldsymbol{x}_2-\boldsymbol{x},\boldsymbol{y}_4)\overline{\check{\mathcal{R}}(\omega,-L,-L_2,\boldsymbol{x}_2,\boldsymbol{y}_3)}\Big]\check{\chi}(\omega,\boldsymbol{y}_2)\overline{\check{\chi}(\omega,\boldsymbol{y}_1)}d\boldsymbol{y}_1 d\boldsymbol{y}_2 d\boldsymbol{y}_3 d\boldsymbol{y}_4. \tag{6.6}$$

Note that, the presence of the reflection operator in the expression for the filter (6.6) modifies the expression for the filter in a way that depends critically on the particular scaling regime considered. We discuss the explicit representation of the filter below.

For completeness we mention that the cross terms can be expressed in terms of the filter $\check{\Lambda}_{\mathrm{t}}^{+}$ defined by (6.2). We have

$$\begin{aligned}\mathcal{V}_{\mathrm{r}}^{+}(s) &= \frac{\mathcal{R}_0}{2\pi}\iint \check{\Lambda}_{\mathrm{t}}^{+}(\omega,\boldsymbol{x};\boldsymbol{x}_1,L_1)\\ &\times\left\{\int \check{\mathcal{R}}(\omega,-L,-L_2,\boldsymbol{x}_2,\boldsymbol{y})\check{\mathcal{T}}(\omega,-L_2,-L_1,\boldsymbol{y},\boldsymbol{x}_1-\boldsymbol{x})d\boldsymbol{y}\right\}d\boldsymbol{x}e^{-i\omega s}d\omega \qquad (6.7)\end{aligned}$$

and

$$\begin{aligned}\mathcal{V}_{\mathrm{r}}^{-}(s) &= \frac{\mathcal{R}_0}{2\pi}\iint \check{\Lambda}_{\mathrm{t}}^{+}(\omega,\boldsymbol{x};\boldsymbol{x}_2,L_2)\\ &\times\left\{\int \check{\mathcal{T}}(\omega,-L_1,-L_2,\boldsymbol{x}_1,\boldsymbol{y})\check{\mathcal{R}}(\omega,-L,-L_2,\boldsymbol{y},\boldsymbol{x}_2-\boldsymbol{x})d\boldsymbol{y}\right\}d\boldsymbol{x}e^{-i\omega s}d\omega. \qquad (6.8)\end{aligned}$$

7. Filters via Wigner transforms. In order to characterize the filter Λ_{t}^{+} we introduce the Wigner transform of the transmission operator defined by

$$\begin{aligned}&W_{\omega}^{\mathrm{T}}(z,\boldsymbol{x},\boldsymbol{x}',\boldsymbol{\kappa},\boldsymbol{\kappa}')\\ &=\iint e^{-i(\boldsymbol{\kappa}\cdot\boldsymbol{y}+\boldsymbol{\kappa}'\cdot\boldsymbol{y}')}\mathbb{E}\Big[\check{\mathcal{T}}\Big(\omega,-z,0,\boldsymbol{x}+\frac{\boldsymbol{y}}{2},\boldsymbol{x}'+\frac{\boldsymbol{y}'}{2}\Big)\overline{\check{\mathcal{T}}\Big(\omega,-z,0,\boldsymbol{x}-\frac{\boldsymbol{y}}{2},\boldsymbol{x}'-\frac{\boldsymbol{y}'}{2}\Big)}\Big]d\boldsymbol{y}d\boldsymbol{y}'\end{aligned}$$

for $z\in(0,L)$. The Wigner transforms satisfy a set of transport equations [12],

$$\begin{aligned}&\frac{\partial W_{\omega}^{\mathrm{T}}}{\partial z}+\frac{\boldsymbol{\kappa}'}{\omega}\cdot\nabla_{\boldsymbol{x}'}W_{\omega}^{\mathrm{T}}\\ &=\frac{\omega^2}{4}\frac{1}{(2\pi)^d}\int\hat{D}(\boldsymbol{u})\big[W_{\omega}^{\mathrm{T}}(z,\boldsymbol{x},\boldsymbol{x}',\boldsymbol{\kappa},\boldsymbol{\kappa}'-\boldsymbol{u})-W_{\omega}^{\mathrm{T}}(z,\boldsymbol{x},\boldsymbol{x}',\boldsymbol{\kappa},\boldsymbol{\kappa}')\big]d\boldsymbol{u},\end{aligned}$$

starting from $W_{\omega}^{\mathrm{T}}(z=0,\boldsymbol{x},\boldsymbol{x}',\boldsymbol{\kappa},\boldsymbol{\kappa}')=(2\pi)^d\delta(\boldsymbol{x}-\boldsymbol{x}')\delta(\boldsymbol{\kappa}+\boldsymbol{\kappa}')$. This system can be integrated [12], and we find the following integral representation for W_{ω}^{T}:

$$W_{\omega}^{\mathrm{T}}(z,\boldsymbol{x},\boldsymbol{x}',\boldsymbol{\kappa},\boldsymbol{\kappa}')=\frac{1}{(2\pi)^d}\iint e^{-i(\boldsymbol{\kappa}'+\boldsymbol{\kappa})\cdot\boldsymbol{a}-i(\boldsymbol{x}'-\boldsymbol{x}+\frac{\boldsymbol{\kappa}}{\omega}z)\cdot\boldsymbol{b}}e^{\frac{\omega^2}{4}\int_0^z D(\boldsymbol{a}+\frac{\boldsymbol{b}}{\omega}z')-D(\boldsymbol{0})dz'}d\boldsymbol{a}d\boldsymbol{b}. \qquad (7.1)$$

The Wigner transform is useful as it allows us to obtain characterizations of second-order moment information for the wave field, and as we will show shortly, this moment information can be used to characterize the Green's function estimate from the correlations.

In order to characterize the filter Λ_{t}^{-} we also introduce the Wigner transform of the reflection operator defined by

$$\begin{aligned}&W_{\omega}^{\mathrm{R}}(z,\boldsymbol{x},\boldsymbol{x}',\boldsymbol{\kappa},\boldsymbol{\kappa}')\\ &=\iint e^{-i(\boldsymbol{\kappa}\cdot\boldsymbol{y}+\boldsymbol{\kappa}'\cdot\boldsymbol{y}')}\mathbb{E}\Big[\check{\mathcal{R}}\Big(\omega,-L,-L+z,\boldsymbol{x}+\frac{\boldsymbol{y}}{2},\boldsymbol{x}'+\frac{\boldsymbol{y}'}{2}\Big)\\ &\qquad\times\overline{\check{\mathcal{R}}\Big(\omega,-L,-L+z,\boldsymbol{x}-\frac{\boldsymbol{y}}{2},\boldsymbol{x}'-\frac{\boldsymbol{y}'}{2}\Big)}\Big]d\boldsymbol{y}d\boldsymbol{y}'.\end{aligned}$$

It satisfies the following set of transport equations:

$$\frac{\partial W_\omega^{\mathrm{R}}}{\partial z}+\frac{\boldsymbol{\kappa}}{\omega}\cdot\nabla_{\boldsymbol{x}}W_\omega^{\mathrm{R}}+\frac{\boldsymbol{\kappa}'}{\omega}\cdot\nabla_{\boldsymbol{x}'}W_\omega^{\mathrm{R}}=\frac{\omega^2}{4(2\pi)^d}\int\hat{D}(\boldsymbol{u})$$
$$\times\Bigg[W_\omega^{\mathrm{R}}\big(z,\boldsymbol{x},\boldsymbol{x}',\boldsymbol{\kappa}-\boldsymbol{u},\boldsymbol{\kappa}'\big)+W_\omega^{\mathrm{R}}\big(z,\boldsymbol{x},\boldsymbol{x}',\boldsymbol{\kappa},\boldsymbol{\kappa}'-\boldsymbol{u}\big)-2W_\omega^{\mathrm{R}}\big(z,\boldsymbol{x},\boldsymbol{x}',\boldsymbol{\kappa},\boldsymbol{\kappa}'\big)$$
$$+2W_\omega^{\mathrm{R}}\Big(z,\boldsymbol{x},\boldsymbol{x}',\boldsymbol{\kappa}-\frac{1}{2}\boldsymbol{u},\boldsymbol{\kappa}'-\frac{1}{2}\boldsymbol{u}\Big)\cos\big(\boldsymbol{u}\cdot(\boldsymbol{x}-\boldsymbol{x}')\big)$$
$$-2W_\omega^{\mathrm{R}}\Big(z,\boldsymbol{x},\boldsymbol{x}',\boldsymbol{\kappa}-\frac{1}{2}\boldsymbol{u},\boldsymbol{\kappa}'+\frac{1}{2}\boldsymbol{u}\Big)\cos\big(\boldsymbol{u}\cdot(\boldsymbol{x}-\boldsymbol{x}')\big)\Bigg]d\boldsymbol{u},$$

starting from $W_\omega^{\mathrm{R}}(z=0,\boldsymbol{x},\boldsymbol{x}',\boldsymbol{\kappa},\boldsymbol{\kappa}')=(2\pi)^d\delta(\boldsymbol{x}-\boldsymbol{x}')\delta(\boldsymbol{\kappa}+\boldsymbol{\kappa}')$.

The filters can now be expressed as

$$\mathbb{E}[\check{\Lambda}_{\mathrm{t}}^{+}(\omega,\boldsymbol{x};\boldsymbol{x}_1,L_1)]$$
$$=\frac{1}{4(2\pi)^{2d}}\iint e^{-i(\boldsymbol{\kappa}\cdot\boldsymbol{x}+\boldsymbol{\kappa}'\cdot(\boldsymbol{y}_1-\boldsymbol{y}_2))}W_\omega^{\mathrm{T}}\left(L_1,\boldsymbol{x}_1-\frac{\boldsymbol{x}}{2},\frac{\boldsymbol{y}_1+\boldsymbol{y}_2}{2},\boldsymbol{\kappa},\boldsymbol{\kappa}'\right)d\boldsymbol{\kappa}d\boldsymbol{\kappa}'$$
$$\times\check{\chi}(\omega,\boldsymbol{y}_2)\overline{\check{\chi}(\omega,\boldsymbol{y}_1)}d\boldsymbol{y}_1d\boldsymbol{y}_2,$$

$$\mathbb{E}[\check{\Lambda}_{\mathrm{t}}^{-}(\omega,\boldsymbol{x};\boldsymbol{x}_2,L_2)]$$
$$=\frac{1}{4(2\pi)^{4d}}\iint e^{i(\boldsymbol{\kappa}\cdot(\boldsymbol{y}_4-\boldsymbol{y}_3)+\boldsymbol{\kappa}'\cdot(\boldsymbol{y}_2-\boldsymbol{y}_1))}W_\omega^{\mathrm{T}}\left(L_2,\frac{\boldsymbol{y}_3+\boldsymbol{y}_4}{2},\frac{\boldsymbol{y}_1+\boldsymbol{y}_2}{2},\boldsymbol{\kappa},\boldsymbol{\kappa}'\right)d\boldsymbol{\kappa}d\boldsymbol{\kappa}'$$
$$\times e^{-i(\boldsymbol{\kappa}_1\cdot\boldsymbol{x}+\boldsymbol{\kappa}_1'\cdot(\boldsymbol{y}_3-\boldsymbol{y}_4))}W_\omega^{\mathrm{R}}\left(L-L_2,\boldsymbol{x}_2-\frac{\boldsymbol{x}}{2},\frac{\boldsymbol{y}_3+\boldsymbol{y}_4}{2},\boldsymbol{\kappa}_1,\boldsymbol{\kappa}_1'\right)d\boldsymbol{\kappa}_1d\boldsymbol{\kappa}_1'$$
$$\times\check{\chi}(\omega,\boldsymbol{y}_2)\overline{\check{\chi}(\omega,\boldsymbol{y}_1)}d\boldsymbol{y}_1d\boldsymbol{y}_2.$$

Here, W_ω^{T} is given by the integral expression in (7.1), and below we shall discuss specific scaling regimes that give explicit expressions for both W_ω^{T} and W_ω^{R}. Indeed, in order to get explicit forms for the filters and characterize the associated resolution scales, or filter support scales, we next consider a particular regime of relatively strong clutter.

8. The strongly cluttered scaling regime. We introduce the correlation length l of the random medium fluctuations, the characteristic frequency ω_c of the source, and the lateral cross section r_0 of the source:

$$C(z,\boldsymbol{x})=\sigma^2C_0\Big(\frac{z}{l},\frac{\boldsymbol{x}}{l}\Big),$$
$$\check{\chi}(\omega,\boldsymbol{y})=\check{\chi}_0\Big(\frac{\omega}{\omega_c},\frac{\boldsymbol{y}}{r_0}\Big),$$

where σ is the standard deviation of the fluctuations of the random medium. We assume that $\check{\chi}_0$ is supported away from the origin in frequency. With this representation we have

$$D(\boldsymbol{x})=\sigma^2lD_0\Big(\frac{\boldsymbol{x}}{l}\Big).$$

We assume also that the auto-correlation function $D_0(\boldsymbol{x})$ is at least twice differentiable at $\boldsymbol{x}=\boldsymbol{0}$, which corresponds to a random medium with relatively smooth fluctuations.

We introduce then the parameter γ defined by

$$\gamma = \frac{1}{d}\frac{1}{(2\pi)^d}\int |\boldsymbol{u}|^2 \hat{D}(\boldsymbol{u})d\boldsymbol{u} = -\frac{1}{d}\Delta D(\mathbf{0}) = -\frac{\sigma^2}{dl}\Delta D_0(\mathbf{0}) = \frac{\sigma^2}{l}\gamma_0, \quad \gamma_0 = -\frac{1}{d}\Delta D_0(\mathbf{0}).$$

We introduce the parameter, depending on (ω, z),

$$\beta(\omega, z) = z\frac{\sigma^2\omega^2 l}{4}, \tag{8.1}$$

which characterizes the *strength of the forward scattering*. We shall then assume a subsequent scaling regime corresponding to relatively strong medium interaction, as given next.

ASSUMPTION 2. $\beta(\omega_c, L_1) \gg 1$.

This scaling may, for instance, be generated by $\sigma \gg 1$, that is, relatively strong clutter fluctuations. We note that this entails for $\omega \sim \omega_c$, $z \sim L_1$

$$\frac{1}{\sqrt{\beta(\omega,z)}}\left(\frac{l}{2\sqrt{\gamma_0}}\right) = \frac{1}{\sqrt{\gamma\omega^2 z}} \ll r_0 \ll \sqrt{\gamma z^3} = \sqrt{\beta(\omega,z)}\left(\frac{2z\sqrt{\gamma_0}}{\omega l}\right). \tag{8.2}$$

We next introduce the *lateral correlation* scale of the transmitted wave field, $\rho_{\mathrm{T}}(z,\omega)$, and the support scale of the *forward cone of wave energy*, $r_{\mathrm{T}}(z)$ [11, 4]:

$$\rho_{\mathrm{T}}(z,\omega) = \frac{4}{\sqrt{\gamma\omega^2 z}}, \qquad r_{\mathrm{T}}(z) = \sqrt{\frac{\gamma z^3}{3}}. \tag{8.3}$$

We will see below that these two quantities determine the behavior of the filter in (6.3). By (8.2) we have

$$\rho_{\mathrm{T}}(z,\omega) \ll r_0 \ll r_{\mathrm{T}}(z).$$

The fact that the lateral correlation length is smaller than the beam radius is responsible for the self-averaging properties of the filters $\check{\Lambda}_{\mathrm{t}}^{\pm}$.

We summarize the scaling assumptions. The main assumption that $\varepsilon \ll 1$ corresponds to very rapid and small medium fluctuations relative to the propagation distance and a high-frequency parabolic source scaling. To get explicit representations for the integral expressions defining the filter Λ_{t}^{+}, in section 9 we assume a strong clutter interaction corresponding to strong forward scattering.

9. Filter asymptotics for the causal Green's function estimate. In Appendix A we derive the following asymptotic expression for $\check{\Lambda}_{\mathrm{t}}^{+}$ that is valid in the strongly cluttered regime.

PROPOSITION 9.1. *Under Assumption* 2, *the filter* $\check{\Lambda}_{\mathrm{t}}^{+}$ *defined by* (6.2) *has the following representation for* $0 < z < L$:

$$\begin{aligned}\check{\Lambda}_{\mathrm{t}}^{+}(\omega,\boldsymbol{x};\boldsymbol{x}_1,z) &\simeq \frac{1}{4}\left(\frac{6}{\pi\gamma z^3}\right)^{d/2}\exp\left(-\frac{\gamma\omega^2 z}{32}|\boldsymbol{x}|^2\right)\exp\left(-\frac{6}{\gamma z^3}|\boldsymbol{x}_1|^2\right)\\ &\quad\times e^{-i\frac{3\omega}{2z}\boldsymbol{x}_1\cdot\boldsymbol{x}}\int|\check{\chi}(\omega,\boldsymbol{y})|^2 d\boldsymbol{y}\\ &= \frac{1}{4}\left(\frac{2}{\pi r_{\mathrm{T}}^2(z)}\right)^{d/2}\exp\left(-\frac{|\boldsymbol{x}|^2}{2\rho_{\mathrm{T}}^2(z,\omega)}\right)\exp\left(-\frac{2|\boldsymbol{x}_1|^2}{r_{\mathrm{T}}^2(z)}\right)\\ &\quad\times e^{-i\sqrt{12}\frac{\boldsymbol{x}}{\rho_{\mathrm{T}}(z,\omega)}\cdot\frac{\boldsymbol{x}_1}{r_{\mathrm{T}}(z)}}\int|\check{\chi}(\omega,\boldsymbol{y})|^2 d\boldsymbol{y}.\end{aligned} \tag{9.1}$$

The filter Λ_{t}^{+} governs the resolution with which the correlation component $\mathcal{V}_{\mathrm{t}}^{+}$ resolves the corresponding empirical Green's function as described in (6.1), that is, the causal Green's function. The support of the filter Λ_{t}^{+} in $\boldsymbol{x}$ determines the resolution in the estimate $\mathcal{V}_{\mathrm{t}}^{+}$ of the Green's function or the amount of blurring in the source coordinate. This is determined by the lateral correlation length $\rho_{\mathrm{T}}(L_1,\omega)$, the lateral coherence scale of the wave field at depth $-L_1$. It also can be seen from (9.1) that the source point $\boldsymbol{x}_1$ must be in the forward cone of wave energy, as determined by $r_{\mathrm{T}}(L_1)$, in order to enable Green's function estimation. We stress here that a relatively sharp Green's function estimate is enabled by a small ρ_T and an enhanced width of the forward cone, both induced by strong medium clutter. We remark that the parameter γ that measures the relative strength of the fluctuations is assumed to be a quantity of order one. As this becomes very large the coherent filter will give high-resolution estimates, but the scale separation becomes smaller, and the estimates will become noisy. Moreover, as the beam width increases with γ, the Itô–Schrödinger model eventually breaks down; this assumes a narrow forward cone and small beam width relative to depth.

The Green's function estimate by $\mathcal{V}_{\mathrm{t}}^{+}$ will also be blurred in time according to the bandwidth of the source trace. We have, using (6.1) and (9.1),

$$\mathcal{V}_{\mathrm{t}}^{+}(s)=\iint\Lambda_{\mathrm{t}}^{+}(t,\boldsymbol{x};\boldsymbol{x}_1,L_1)\mathcal{T}(s-t,-L_2,-L_1,\boldsymbol{x}_2,\boldsymbol{x}_1-\boldsymbol{x})d\boldsymbol{x}dt \tag{9.2}$$

for

$$\begin{aligned}\Lambda_{\mathrm{t}}^{+}(t,\boldsymbol{x};\boldsymbol{x}_1,z)&=\frac{1}{4}\Big(\frac{2}{\pi r_{\mathrm{T}}^2(z)}\Big)^{d/2}\exp\Big(-\frac{2|\boldsymbol{x}_1|^2}{r_{\mathrm{T}}^2(z)}\Big)\\&\quad\times\frac{\tilde\rho_{\mathrm{T}}(z)}{\sqrt{2\pi}|\boldsymbol{x}|}\int\exp\Big(-\frac{\tilde\rho_{\mathrm{T}}^2(z)s^2}{2|\boldsymbol{x}|^2}\Big)\,\Phi\big(t+\theta_{\mathrm{T}}(\boldsymbol{x},\boldsymbol{x}_1,z)-s\big)ds.\end{aligned} \tag{9.3}$$

Here, we used the notation

$$\Phi(s)=\iint\chi(t,\boldsymbol{y})\chi(t+s,\boldsymbol{y})d\boldsymbol{y}dt,\quad\tilde\rho_{\mathrm{T}}(z)=\frac{4}{\sqrt{\gamma z}},$$
$$\theta_{\mathrm{T}}(\boldsymbol{x},\boldsymbol{x}_1,z)=\sqrt{12}\frac{\boldsymbol{x}}{\tilde\rho_{\mathrm{T}}(z)}\cdot\frac{\boldsymbol{x}_1}{r_{\mathrm{T}}(z)}.$$

Thus, the cross correlation gives a blurred Green's function, corresponding to smoothing in time and source point and with a slight time shift for contributions with lateral offsets. The spatial source point focusing follows from the increase of support in the time smoothing with increased lateral offset.

In the case when χ has a *narrow bandwidth* and carrier frequency ω_c, we have

$$\Lambda_{\mathrm{t}}^{+}(t,\boldsymbol{x};\boldsymbol{x}_1,z)=\frac{1}{4}\Big(\frac{2}{\pi r_{\mathrm{T}}^2(z)}\Big)^{d/2}\exp\Big(-\frac{|\boldsymbol{x}|^2}{2\rho_{\mathrm{T}}^2(z,\omega_c)}\Big)\exp\Big(-\frac{2|\boldsymbol{x}_1|^2}{r_{\mathrm{T}}^2(z)}\Big)\,\Phi\big(t+\theta_{\mathrm{T}}(\boldsymbol{x},\boldsymbol{x}_1,z)\big). \tag{9.4}$$

Finally, if we also assume a *relatively small offset*, $|\boldsymbol{x}_1|\ll r_{\mathrm{T}}(L_1)$, we have

$$\Lambda_{\mathrm{t}}^{+}(t,\boldsymbol{x};\boldsymbol{x}_1,L_1)=\frac{1}{4}\Big(\frac{2}{\pi r_{\mathrm{T}}^2(L_1)}\Big)^{d/2}\exp\Big(-\frac{|\boldsymbol{x}|^2}{2\rho_{\mathrm{T}}^2(L_1,\omega_c)}\Big)\,\Phi(t). \tag{9.5}$$

In conclusion, the Green's function in (9.2) is blurred in time according to the autocorrelation of the source time trace, and in space according to the Gaussian with

support determined by the spatial decorrelation length of the wave field at $z = -L_1$ when emanating from a point source at $z = 0$ and with carrier ω_c. There is also a damping of the filter with the widening of the forward cone. We recall that this final description holds under the assumption that $\boldsymbol{x}_1$ is within the forward cone of wave energy, or $|\boldsymbol{x}_1| < r_{\mathrm{T}}(L_1)$.

10. Filter asymptotics for the anticausal Green's function estimate. We now turn to the filter Λ_{t}^- that gives the anticausal contribution in (6.4). We shall here consider the regime of strong and rapid clutter. In this case we assume the following.

ASSUMPTION 3. $r_0 \gg l$, $\omega_c r_0 l = \mathcal{O}(L)$.

We note that, in the random medium case, diffractive effects are of order one when $\omega_c r_0 l \sim L$. This is when the Rayleigh length associated with the Fresnel length, $\sqrt{r_0 l}$, is of order the depth of the slab. Note that in this configuration the random medium fluctuations give an earlier onset of diffractive effects than in the homogeneous case. In this case we show in Appendix B the following asymptotic representation for the filter $\check{\Lambda}_t^-$.

PROPOSITION 10.1. *Under Assumptions* 2–3*, the filter* $\check{\Lambda}_{\mathrm{t}}^-$ *defined by* (6.6) *has the representation*

$$\check{\Lambda}_t^-(\omega, \boldsymbol{x}; \boldsymbol{x}_1, z, L) \simeq \check{\Lambda}_t^+(\omega, \boldsymbol{x}; \boldsymbol{x}_1, 2L - z). \tag{10.1}$$

Therefore, the spatial resolution for the filter with a relatively deep reflector (i.e., $L \gg z$) is as if the field propagated in a medium corresponding to twice the travel distance to the reflector at $-L$ and acquires the corresponding shortened spatial decorrelation length. Note that with a deep reflector, with L much larger than L_1, the filter Λ_t^+ gives much better resolution than the filter Λ_t^-, at the cost of a reduced amplitude. In this case the cross correlation presents a strong asymmetry between the causal and anticausal components.

In the special case that $L \simeq z$ we have

$$\Lambda_{\mathrm{t}}^-(t, \boldsymbol{x}; \boldsymbol{x}_1, z, L) \simeq \Lambda_{\mathrm{t}}^+(t, \boldsymbol{x}; \boldsymbol{x}_1, L),$$

so that the filters coincide if the interface is located just below both of the points of observation. In this case the cross correlation presents a symmetry between the causal and anticausal components.

11. Horizontal moveout case. We consider here the situation when both the measurements are taken at the surface $z = 0$. In this case the observations can be derived from (6.4):

$$\begin{aligned}\mathcal{V}_{\mathrm{t}}^-(s) &= \frac{\mathcal{R}_0^2}{2\pi} \iint \check{\Lambda}_{\mathrm{t}}^-(\omega, \boldsymbol{x}; \boldsymbol{x}_2, 0, L) \check{\mathcal{T}}(\omega, 0, 0, \boldsymbol{x}_1, \boldsymbol{x}_2 - \boldsymbol{x}) d\boldsymbol{x} e^{-i\omega s} d\omega \\ &= \mathcal{R}_0^2 \Lambda_{\mathrm{t}}^-(s, \boldsymbol{x}_2 - \boldsymbol{x}_1; \boldsymbol{x}_2, 0, L).\end{aligned}$$

Therefore, by varying the horizontal offset for the two measurement points, we can estimate the filter, as a function of midpoint, offset (or $\boldsymbol{x}_1, \boldsymbol{x}_2$ as in (11.2)), and time. In the strongly cluttered scaling regime the filter function gives a concise parameterization for the effective parameters associated with the medium that we can estimate. Under Assumptions 1, 2, and 3, and assuming a narrow bandwidth for χ_0, we have,

using (9.4) and (10.1),

(11.1)
$$
\begin{aligned}
&\check{\Lambda}_{\mathrm{t}}^{-}(s,\boldsymbol{x}_2-\boldsymbol{x}_1;\boldsymbol{x}_2,0,L)\\
&\simeq \frac{1}{4}\left(\frac{3}{4\pi\gamma L^3}\right)^{d/2}\exp\left(-\frac{\gamma\omega_c^2 L}{16}|\boldsymbol{x}_1-\boldsymbol{x}_2|^2\right)\\
&\qquad\times\exp\left(-\frac{3}{4\gamma L^3}|\boldsymbol{x}_2|^2\right)\Phi\big(s+\theta_{\mathrm{R}}(\boldsymbol{x}_2-\boldsymbol{x}_1,\boldsymbol{x}_2,L)\big)\\
&=\frac{1}{4}\left(\frac{2}{\pi r_{\mathrm{R}}^2(L)}\right)^{d/2}\exp\left(-\frac{|\boldsymbol{x}_1-\boldsymbol{x}_2|^2}{2\rho_{\mathrm{R}}^2(L,\omega_c)}\right)\exp\left(-\frac{2|\boldsymbol{x}_2|^2}{r_{\mathrm{R}}^2(L)}\right)\Phi\big(s+\theta_{\mathrm{R}}(\boldsymbol{x}_2-\boldsymbol{x}_1,\boldsymbol{x}_2,L)\big)\\
&\simeq\frac{1}{4}\left(\frac{2}{\pi r_{\mathrm{R}}^2(L)}\right)^{d/2}\exp\left(-\frac{|\boldsymbol{x}_{\mathrm{off}}|^2}{2\rho_{\mathrm{R}}^2(L,\omega_c)}\right)\exp\left(-\frac{2|\boldsymbol{x}_{\mathrm{mid}}|^2}{r_{\mathrm{R}}^2(L)}\right)\Phi\big(s+\theta_{\mathrm{R}}(-\boldsymbol{x}_{\mathrm{off}},\boldsymbol{x}_{\mathrm{mid}},L)\big),
\end{aligned}
$$

where we have used the notation

$$
\boldsymbol{x}_{\mathrm{mid}}=\frac{\boldsymbol{x}_1+\boldsymbol{x}_2}{2},\qquad \boldsymbol{x}_{\mathrm{off}}=\boldsymbol{x}_1-\boldsymbol{x}_2, \tag{11.2}
$$

and

$$
\rho_{\mathrm{R}}(L,\omega_c)=\frac{4}{\sqrt{2\omega_c^2\gamma L}},\qquad r_{\mathrm{R}}(z)=\sqrt{\frac{8\gamma L^3}{3}}.
$$

Finally, we also have here

$$
\theta_{\mathrm{R}}(\boldsymbol{x},\boldsymbol{x}_1,L)=\sqrt{12}\frac{\boldsymbol{x}}{\tilde{\rho}_{\mathrm{R}}(L)}\cdot\frac{\boldsymbol{x}_1}{r_{\mathrm{R}}(L)},\qquad \tilde{\rho}_{\mathrm{R}}(L)=\frac{4}{\sqrt{2\gamma L}}.
$$

In the case that we have measurements along a line through the center of the source (the origin in our coordinate system), we can then observe, using various offsets and centerpoints, two parameters that encapsulate the "measurable" medium information:

$$
\mathcal{P}_1=\gamma L,\qquad \mathcal{P}_2=\gamma L^3.
$$

The point is that, measuring both the wave field decorrelation length and the energy cone spreading, we can construct an estimate for depth without prior information about the medium microstructure. The important assumption here is that we have a statistically homogeneous medium; we comment on the more general case below. This is exactly the information the cross correlations convey in the regime that we consider. We stress that in a situation with finite scales the filter observations will not be perfectly stable with respect to the statistical distribution of the random medium. The observations at many offsets, centerpoints, and possibly also carrier frequencies will be needed to get robust estimates of these parameters. The important point now is that we can obtain an estimate of the depth to the reflector and the medium correlation parameter from estimates $\hat{\mathcal{P}}_1$ and $\hat{\mathcal{P}}_2$:

$$
\hat{L}=\sqrt{\frac{\hat{\mathcal{P}}_2}{\hat{\mathcal{P}}_1}},\qquad \hat{\gamma}=\sqrt{\frac{\hat{\mathcal{P}}_1^3}{\hat{\mathcal{P}}_2}}. \tag{11.3}
$$

The construction of the estimates $\hat{\mathcal{P}}_1$, $\hat{\mathcal{P}}_2$ needs to be tuned to the particular configuration at hand. However, our scaling limit analysis gives guidelines for optimal design

of measurement configuration for constructing such estimates. We also remark that this is just the starting point for a more elaborate analysis for cases where the medium background varies smoothly so that the medium fluctuations are locally stationary. Note that if we assume a general smooth background, then in our parabolic scaling we will have smooth order one variations with respect to depth but slow variations with respect to the lateral coordinates. Thus, this is a perturbation of the case with depth-dependent background only. If we next consider two measurements with large offset relative to the center point and possibly also large offset in between them, then in fact the effective medium parameters along the "rays" between the source point and the points of observation can be estimated. This is a set-up for estimating fabric as well as deterministic discontinuities. Let us consider first the situation addressed above, in which the background velocity is constant. Then in the process of estimating the reflector depth function, $L(\boldsymbol{x})$, we also need to estimate the location-dependent correlation parameter map of the medium in the overburden, $\gamma(z, \boldsymbol{x})$. We stress that this correlation map is of importance, as it may relate to the geological fabric. Note that if in addition the background velocity varies smoothly, then this estimation needs to be carried out jointly with a "velocity analysis." Our paper presents the first step towards imaging involving the joint estimate of the microstructure correlation function and the local velocity function based on both correlations and travel time estimates. Our method is particularly effective in the case with relatively strong medium and measurement noise: the recorded signals are then cluttered, and formation of cross correlations is needed to stabilize the data.

12. Discussion. We have presented an analysis for partly coherent body waves generated by a (teleseismic) wave packet remotely incident on a slab (the crust) containing a medium consisting of a deterministic component and a random field. We assume a parabolic scaling of the incident wave packet which is coupled to the scaling of the random fluctuations. In practical situations, such an incident wave packet may be synthesized from given observed data. The deterministic component consists, here, of a planarly layered medium, but it can be generalized to contain conormal singularities (discontinuities) combined with smooth wave speed variations. To obtain information about the deterministic medium component, one needs to consider "field-field" cross correlations. We have shown that these cross correlations are characterized by a statistically stable transformation (blurring filter) applied to the transmission operator given by an Itô–Schrödinger diffusion model, which we interpret as the Green's function between two points. The blurring transformation contains information about the statistics of the random fluctuations. If the points are taken purely transverse to the propagation direction of the wave packet in the deterministic component, the blurring significantly increases, which is consistent with the usual stationary phase arguments. In principle, incident packets also can be summed to form a point source, to represent local seismicity.

Appendix A. Correlation filter in strongly cluttered narrow bandwidth regime. In this appendix we derive the expression (9.1) for the filter. To get an explicit expression of the filter Λ_{t}^{+} we need an expression for W_{ω}^{T} in the strongly cluttered regime. With Assumption 2 we obtain

$$W_{\omega}^{\mathrm{T}}(z, \boldsymbol{x}, \boldsymbol{x}', \boldsymbol{\kappa}, \boldsymbol{\kappa}') \simeq \frac{1}{(2\pi)^d} \iint e^{-i(\boldsymbol{\kappa}'+\boldsymbol{\kappa})\cdot\boldsymbol{a} - i(\boldsymbol{x}'-\boldsymbol{x}+\frac{\boldsymbol{\kappa}}{\omega}z)\cdot\boldsymbol{b}} e^{-\frac{\gamma\omega^2}{8}\left(|\boldsymbol{a}|^2 z + \frac{\boldsymbol{a}\cdot\boldsymbol{b}}{\omega} z^2 + \frac{1}{3}\frac{|\boldsymbol{b}|^2}{\omega^2} z^3\right)} d\boldsymbol{a} d\boldsymbol{b}. \tag{A.1}$$

Taking an inverse Fourier transform, we find that the cross correlation function of the kernel of transmission operator is

$$\mathbb{E}\Big[\check{\mathcal{T}}\Big(\omega,-z,0,\boldsymbol{x}+\frac{\boldsymbol{y}}{2},\boldsymbol{x}'+\frac{\boldsymbol{y}'}{2}\Big)\overline{\check{\mathcal{T}}\Big(\omega,-z,0,\boldsymbol{x}-\frac{\boldsymbol{y}}{2},\boldsymbol{x}'-\frac{\boldsymbol{y}'}{2}\Big)}\Big] \simeq \Big(\frac{\omega}{2\pi z}\Big)^d e^{i\frac{\omega}{z}(\boldsymbol{x}'-\boldsymbol{x})\cdot(\boldsymbol{y}'-\boldsymbol{y})} e^{-\frac{\gamma\omega^2 z}{8}\left(\frac{1}{3}|\boldsymbol{y}'+\frac{1}{2}\boldsymbol{y}|^2+\frac{1}{4}|\boldsymbol{y}|^2\right)}. \tag{A.2}$$

Using the self-averaging property, (6.3), and (A.2), we find

$$\check{\Lambda}_{\rm t}^{+}(\omega,\boldsymbol{x};\boldsymbol{x}_1,z) = \frac{1}{4}\iint\Big(\frac{\omega}{2\pi z}\Big)^d e^{i\frac{\omega}{2z}(\boldsymbol{y}_1+\boldsymbol{y}_1'+\boldsymbol{x}-2\boldsymbol{x}_1)\cdot(\boldsymbol{y}_1-\boldsymbol{y}_1'+\boldsymbol{x})} e^{-\frac{\gamma\omega^2 z}{8}\left(\frac{1}{3}|\boldsymbol{y}_1-\boldsymbol{y}_1'-\frac{1}{2}\boldsymbol{x}|^2+\frac{1}{4}|\boldsymbol{x}|^2\right)} \times\check{\chi}(\omega,\boldsymbol{y}_1)\overline{\check{\chi}(\omega,\boldsymbol{y}_1')}d\boldsymbol{y}_1 d\boldsymbol{y}_1'.$$

Using the first inequality in (8.2), we obtain

$$\begin{aligned}
&\check{\Lambda}_{\rm t}^{+}(\omega,\boldsymbol{x};\boldsymbol{x}_1,z)\\
&\simeq \frac{1}{4}\iint\Big(\frac{\omega}{2\pi z}\Big)^d e^{i\frac{\omega}{z}\left(\boldsymbol{z}_1+\frac{1}{2}\boldsymbol{x}-\boldsymbol{x}_1\right)\cdot\left(\boldsymbol{z}_2+\boldsymbol{x}\right)} e^{-\frac{\gamma\omega^2 z}{8}\left(\frac{1}{3}|\boldsymbol{z}_2-\frac{1}{2}\boldsymbol{x}|^2+\frac{1}{4}|\boldsymbol{x}|^2\right)}|\check{\chi}(\omega,\boldsymbol{z}_1)|^2 d\boldsymbol{z}_1 d\boldsymbol{z}_2\\
&\simeq \frac{1}{4}\iint\Big(\frac{\omega}{2\pi z}\Big)^d e^{i\frac{\omega}{z}\left(\boldsymbol{z}_1-\boldsymbol{x}_1\right)\cdot\left(\boldsymbol{z}_2+\frac{3}{2}\boldsymbol{x}\right)} e^{-\frac{\gamma\omega^2 z}{8}\left(\frac{1}{3}|\boldsymbol{z}_2|^2+\frac{1}{4}|\boldsymbol{x}|^2\right)}|\check{\chi}(\omega,\boldsymbol{z}_1)|^2 d\boldsymbol{z}_1 d\boldsymbol{z}_2\\
&= \frac{1}{4}\Big(\frac{6}{\pi\gamma z^3}\Big)^{d/2}\exp\left(-\frac{\gamma\omega^2 z}{32}|\boldsymbol{x}|^2\right) e^{-i\frac{3\omega}{2z}\boldsymbol{x}_1\cdot\boldsymbol{x}}\int e^{i\frac{3\omega}{2z}\boldsymbol{z}_1\cdot\boldsymbol{x}} e^{-\frac{6}{\gamma z^3}|\boldsymbol{z}_1-\boldsymbol{x}_1|^2}|\check{\chi}(\omega,\boldsymbol{z}_1)|^2 d\boldsymbol{z}_1.
\end{aligned}$$

Then using the second inequality in (8.2), we find

$$\begin{aligned}
&\check{\Lambda}_{\rm t}^{+}(\omega,\boldsymbol{x};\boldsymbol{x}_1,z)\\
&\simeq \frac{1}{4}\Big(\frac{6}{\pi\gamma z^3}\Big)^{d/2}\exp\left(-\frac{\gamma\omega^2 z}{32}|\boldsymbol{x}|^2\right)\exp\left(-\frac{6}{\gamma z^3}|\boldsymbol{x}_1|^2\right) e^{-i\frac{3\omega}{2z}\boldsymbol{x}_1\cdot\boldsymbol{x}}\int|\check{\chi}(\omega,\boldsymbol{y})|^2 d\boldsymbol{y}.
\end{aligned}$$

Appendix B. Correlation filter in the backscattering case. We consider the filter $\check{\Lambda}_{\rm t}^{-}$ and derive the representation (10.1). Using the self-averaging property, the filter is given by (6.6):

$$\begin{aligned}
\check{\Lambda}_{\rm t}^{-}(\omega,\boldsymbol{x};\boldsymbol{x}_1,z,L) &= \frac{1}{4}\iint\mathbb{E}\big[\check{\mathcal{T}}(\omega,-z,0,\boldsymbol{y}_4,\boldsymbol{y}_2)\overline{\check{\mathcal{T}}(\omega,-z,0,\boldsymbol{y}_3,\boldsymbol{y}_1)}\big]\\
&\times\mathbb{E}\Big[\check{\mathcal{R}}(\omega,-L,-z,\boldsymbol{x}_1-\boldsymbol{x},\boldsymbol{y}_4)\overline{\check{\mathcal{R}}(\omega,-L,-z,\boldsymbol{x}_1,\boldsymbol{y}_3)}\Big]\check{\chi}(\omega,\boldsymbol{y}_2)\overline{\check{\chi}(\omega,\boldsymbol{y}_1)}d\boldsymbol{y}_1 d\boldsymbol{y}_2 d\boldsymbol{y}_3 d\boldsymbol{y}_4\\
&= \iint\mathbb{E}\Big[\check{\mathcal{R}}(\omega,-L,-z,\boldsymbol{x}_1-\boldsymbol{x},\boldsymbol{y}_1)\overline{\check{\mathcal{R}}(\omega,-L,-z,\boldsymbol{x}_1,\boldsymbol{y}_1')}\Big]\check{\Lambda}_{\rm t}^{+}(\omega,\boldsymbol{y}_1'-\boldsymbol{y}_1;\boldsymbol{y}_1',z)d\boldsymbol{y}_1 d\boldsymbol{y}_1'.
\end{aligned} \tag{B.1}$$

In terms of center and offset coordinates this can be written as

$$\begin{aligned}
\check{\Lambda}_{\rm t}^{-}\Big(\omega,-\boldsymbol{y};\boldsymbol{x}-\frac{\boldsymbol{y}}{2},z,L\Big) &= \iint\mathbb{E}\Big[\check{\mathcal{R}}\Big(\omega,-L,-z,\boldsymbol{x}+\frac{\boldsymbol{y}}{2},\boldsymbol{y}_1\Big)\overline{\check{\mathcal{R}}\Big(\omega,-L,-z,\boldsymbol{x}-\frac{\boldsymbol{y}}{2},\boldsymbol{y}_1'\Big)}\Big]\\
&\quad\times\check{\Lambda}_{\rm t}^{+}(\omega,\boldsymbol{y}_1'-\boldsymbol{y}_1;\boldsymbol{y}_1',z)d\boldsymbol{y}_1 d\boldsymbol{y}_1'\\
&= (2\pi)^{-2d}\iint e^{i(\boldsymbol{\kappa}\cdot\boldsymbol{y}+\boldsymbol{\kappa}'\cdot(\boldsymbol{y}_1-\boldsymbol{y}_1'))}W_\omega^{\rm R}\Big(L-z,\boldsymbol{x},\frac{\boldsymbol{y}_1+\boldsymbol{y}_1'}{2},\boldsymbol{\kappa},\boldsymbol{\kappa}'\Big)\\
&\quad\times\check{\Lambda}_{\rm t}^{+}(\omega,\boldsymbol{y}_1'-\boldsymbol{y}_1;\boldsymbol{y}_1',z)d\boldsymbol{\kappa}d\boldsymbol{\kappa}'d\boldsymbol{y}_1 d\boldsymbol{y}_1'.
\end{aligned}$$

From (C.1) and (C.2) we have

$$W_\omega^{\mathrm{R}}(z,\boldsymbol{x},\boldsymbol{x}',\boldsymbol{\kappa},\boldsymbol{\kappa}') = \left(\frac{l}{2}\right)^d \int e^{i\boldsymbol{\kappa}''\cdot(\boldsymbol{x}'-\boldsymbol{x})} e^{iz(\boldsymbol{\kappa}-\boldsymbol{\kappa}')\cdot\boldsymbol{\kappa}''/\omega} \times \mathcal{V}^{\mathrm{R}}\left(1, \frac{l(\boldsymbol{\kappa}+\boldsymbol{\kappa}')}{2}, l(\boldsymbol{\kappa}-\boldsymbol{\kappa}'), l\boldsymbol{\kappa}''; \alpha(\omega,z), \beta(\omega,z)\right) d\boldsymbol{\kappa}'',$$

with $\alpha(\omega,z) = z/(\omega l^2)$ characterizing the diffractive effects and $\beta(\omega,z) = z\sigma^2\omega^2 l/4$ characterizing the strength of forward scattering. We then get

$$\begin{aligned}
&\check{\Lambda}_{\mathrm{t}}^-\left(\omega, -\boldsymbol{y}; \boldsymbol{x} - \frac{\boldsymbol{y}}{2}, z, L\right)\\
&= (2\pi)^{-2d}\left(\frac{l}{2}\right)^d \iint e^{i(\boldsymbol{\kappa}\cdot\boldsymbol{y}+\boldsymbol{\kappa}'\cdot(\boldsymbol{y}_1-\boldsymbol{y}_1'))} e^{i\boldsymbol{\kappa}''\cdot((\boldsymbol{y}_1+\boldsymbol{y}_1')/2-\boldsymbol{x})} e^{i(L-z)(\boldsymbol{\kappa}-\boldsymbol{\kappa}')\cdot\boldsymbol{\kappa}''/\omega}\\
&\quad\times \mathcal{V}^{\mathrm{R}}\left(1, \frac{l(\boldsymbol{\kappa}+\boldsymbol{\kappa}')}{2}, l(\boldsymbol{\kappa}-\boldsymbol{\kappa}'), l\boldsymbol{\kappa}''; \alpha(\omega,L-z), \beta(\omega,L-z)\right)\\
&\quad\times \check{\Lambda}_{\mathrm{t}}^+(\omega, \boldsymbol{y}_1'-\boldsymbol{y}_1; \boldsymbol{y}_1', z) d\boldsymbol{\kappa}'' d\boldsymbol{\kappa} d\boldsymbol{\kappa}' d\boldsymbol{y}_1 d\boldsymbol{y}_1'\\
&= (2\pi)^{-2d}\left(\frac{1}{2l^2}\right)^d \iint e^{i((\boldsymbol{q}+\boldsymbol{r}/2)\cdot\boldsymbol{y}/l + (\boldsymbol{q}-\boldsymbol{r}/2)\cdot(\boldsymbol{y}_1-\boldsymbol{y}_1')/l)} e^{i\boldsymbol{s}\cdot((\boldsymbol{y}_1+\boldsymbol{y}_1')/2-\boldsymbol{x})/l} e^{i(L-z)\boldsymbol{r}\cdot\boldsymbol{s}/(\omega l^2)}\\
&\quad\times \mathcal{V}^{\mathrm{R}}\Big(1, \boldsymbol{q}, \boldsymbol{r}, \boldsymbol{s}; \alpha(\omega,L-z), \beta(\omega,L-z)\Big) \check{\Lambda}_{\mathrm{t}}^+(\omega, \boldsymbol{y}_1'-\boldsymbol{y}_1; \boldsymbol{y}_1', z) d\boldsymbol{q} d\boldsymbol{r} d\boldsymbol{s} d\boldsymbol{y}_1 d\boldsymbol{y}_1'.
\end{aligned}$$

Taking the Fourier transform of the filter in its second and third variables, we get

$$\begin{aligned}
\check{\Lambda}_{\mathrm{t}}^-(\omega, -\boldsymbol{y}; \boldsymbol{x}-\boldsymbol{y}/2, z, L) &= ((2\pi)^2 2l^2)^{-d} \iint e^{i(\boldsymbol{q}+\boldsymbol{r}/2)\cdot\boldsymbol{y}/l} e^{-i\boldsymbol{s}\cdot\boldsymbol{x}/l} e^{i\alpha(\omega,L-z)\boldsymbol{r}\cdot\boldsymbol{s}}\\
&\quad\times \mathcal{V}^{\mathrm{R}}\Big(1, \boldsymbol{q}, \boldsymbol{r}, \boldsymbol{s}; \alpha(\omega,L-z), \beta(\omega,L-z)\Big) \hat{\Lambda}_{\mathrm{t}}^+(\omega, (\boldsymbol{r}/2-\boldsymbol{s}/2-\boldsymbol{q})/l; \boldsymbol{s}/l, z) d\boldsymbol{q} d\boldsymbol{r} d\boldsymbol{s},
\end{aligned}$$

with

$$\hat{\Lambda}_{\mathrm{t}}^+(\omega, \boldsymbol{\kappa}_1; \boldsymbol{\kappa}_2, z) = \iint \check{\Lambda}_{\mathrm{t}}^+(\omega, \boldsymbol{y}_1; \boldsymbol{y}_2, z) e^{i(\boldsymbol{\kappa}_1\cdot\boldsymbol{y}_1 + \boldsymbol{\kappa}_2\cdot\boldsymbol{y}_2)} d\boldsymbol{y}_1 d\boldsymbol{y}_2.$$

Using the change of variables $\boldsymbol{s} \mapsto \boldsymbol{s}/(2\alpha)$ and $\boldsymbol{r} \mapsto \boldsymbol{r} + 2\boldsymbol{q}$, we get

$$\begin{aligned}
\check{\Lambda}_{\mathrm{t}}^-\left(\omega, -\boldsymbol{y}; \boldsymbol{x}-\frac{\boldsymbol{y}}{2}, z, L\right) &= ((4\pi)^2 \alpha(\omega,L-z) l^2)^{-d} \iint e^{i(2\boldsymbol{q}+\boldsymbol{r}/2)\cdot\boldsymbol{y}/l} e^{-i\boldsymbol{s}\cdot\boldsymbol{x}/(2l\alpha(\omega,L-z))}\\
&\quad\times e^{i(\boldsymbol{r}/2+\boldsymbol{q})\cdot\boldsymbol{s}} \mathcal{V}^{\mathrm{R}}\left(1, \boldsymbol{q}, \boldsymbol{r}+2\boldsymbol{q}, \frac{\boldsymbol{s}}{2\alpha(\omega,L-z)}; \alpha(\omega,L-z), \beta(\omega,L-z)\right)\\
&\quad\times \hat{\Lambda}_{\mathrm{t}}^+\left(\omega, \frac{\boldsymbol{r}/2-\boldsymbol{s}/(4\alpha(\omega,L-z))}{l}; \frac{\boldsymbol{s}}{2l\alpha(\omega,L-z)}, z\right) d\boldsymbol{q} d\boldsymbol{r} d\boldsymbol{s}.
\end{aligned}$$

Next we use Lemma C.1 to get

$$\begin{aligned}
\check{\Lambda}_{\mathrm{t}}^-\left(\omega, -\boldsymbol{y}; \boldsymbol{x}-\frac{\boldsymbol{y}}{2}, z, L\right) &= (4(2\pi)^3 \alpha(\omega,L-z) l^2)^{-d} \iint e^{i(2\boldsymbol{q}+\boldsymbol{r}/2)\cdot\boldsymbol{y}/l} e^{-i\boldsymbol{s}\cdot\boldsymbol{x}/(2l\alpha(\omega,L-z))}\\
&\quad\times e^{i(\boldsymbol{r}/2+\boldsymbol{q})\cdot\boldsymbol{s}} e^{-i\boldsymbol{q}\cdot\boldsymbol{u}} e^{\beta(\omega,L-z)\int_{-1}^1 D_0(\frac{\boldsymbol{u}}{2}+\frac{\boldsymbol{s}}{2}\zeta) - D_0(\boldsymbol{0}) d\zeta}\\
&\quad\times \hat{\Lambda}_{\mathrm{t}}^+\left(\omega, \frac{\boldsymbol{r}/2-\boldsymbol{s}/(4\alpha(\omega,L-z))}{l}; \frac{\boldsymbol{s}}{2l\alpha(\omega,L-z)}, z\right) d\boldsymbol{q} d\boldsymbol{r} d\boldsymbol{s} d\boldsymbol{u}.
\end{aligned}$$

Integrating in $\boldsymbol{q}$ and evaluating the resulting Dirac distribution, we get

$$\check{\Lambda}_{\mathrm{t}}^{-}\left(\omega,-\boldsymbol{y};\boldsymbol{x}-\frac{\boldsymbol{y}}{2},z,L\right)=(4(2\pi)^2\alpha(\omega,L-z)l^2)^{-d}\iint e^{i\boldsymbol{r}\cdot(\boldsymbol{s}+\boldsymbol{y}/l)/2}e^{-i\boldsymbol{s}\cdot\boldsymbol{x}/(2l\alpha(\omega,L-z))}$$
$$\times\, e^{2\beta\int_0^1 D_0(\boldsymbol{y}/l+\boldsymbol{s}\zeta)-D_0(\boldsymbol{0})d\zeta}\hat{\Lambda}_{\mathrm{t}}^{+}\left(\omega,\frac{\boldsymbol{r}/2-\boldsymbol{s}/(4\alpha(\omega,L-z))}{l};\frac{\boldsymbol{s}}{2l\alpha(\omega,L-z)},z\right)d\boldsymbol{r}d\boldsymbol{s}.$$

Finally, we then get

$$\check{\Lambda}_{\mathrm{t}}^{-}\left(\omega,-\boldsymbol{y};\boldsymbol{x}-\frac{\boldsymbol{y}}{2},z,L\right)=(4\pi\alpha(\omega,L-z)l)^{-d}\int e^{\frac{i|\boldsymbol{s}|^2}{4\alpha(\omega,L-z)}}e^{-\frac{i\boldsymbol{s}\cdot(\boldsymbol{x}-\boldsymbol{y}/2)}{2l\alpha(\omega,L-z)}}$$
$$\times\, e^{2\beta\int_0^1 D_0(\frac{\boldsymbol{y}}{l}+\boldsymbol{s}\zeta)-D_0(\boldsymbol{0})d\zeta}\tilde{\Lambda}_{\mathrm{t}}^{+}\left(\omega,-l\boldsymbol{s}-\boldsymbol{y};\frac{\boldsymbol{s}}{2l\alpha(\omega,L-z)},z\right)d\boldsymbol{s} \tag{B.2}$$

for

$$\tilde{\Lambda}_{\mathrm{t}}^{+}(\omega,\boldsymbol{y}_1;\boldsymbol{\kappa}_2,z)=\int\check{\Lambda}_{\mathrm{t}}^{+}(\omega,\boldsymbol{y}_2;\boldsymbol{y}_2,z)e^{i\boldsymbol{\kappa}_2\cdot\boldsymbol{y}_2}d\boldsymbol{y}_2=\frac{1}{(2\pi)^d}\int\hat{\Lambda}_{\mathrm{t}}^{+}(\omega,\boldsymbol{\kappa}_1;\boldsymbol{\kappa}_2,z)e^{-i\boldsymbol{\kappa}_1\cdot\boldsymbol{y}_2}d\boldsymbol{\kappa}_1.$$

We next show that this expression for the filter in fact could have been obtained by using the statistics for the transmission operator rather than those of the reflection operator, however, at a scaled depth. Specifically, the "effective depth" is doubled, corresponding to the two-way "independent" passages of the bottom part of the slab. Albeit very intuitive, this is a deep result that builds on the Itô–Schrödinger equations and the specific scaling assumptions that we make. It is not valid in general. Important physical phenomena (such as weak localization or enhanced backscattering phenomena) correspond exactly to the situation when this "independence" property fails. The significance of such configurations from the point of view of imaging in our setting will be treated elsewhere. In view of (B.1) we then define

$$\begin{aligned}\check{\mathcal{H}}_{\mathrm{t}}^{-}(\omega,\boldsymbol{x};\boldsymbol{x}_1,z,L)&=\frac{1}{4}\iint\mathbb{E}\Big[\check{\mathcal{T}}(\omega,-z,0,\boldsymbol{y}_4,\boldsymbol{y}_2)\overline{\check{\mathcal{T}}(\omega,-z,0,\boldsymbol{y}_3,\boldsymbol{y}_1)}\Big]\\&\times\mathbb{E}\Big[\check{\mathcal{T}}(\omega,-2L+z,-z,\boldsymbol{x}_1-\boldsymbol{x},\boldsymbol{y}_4)\overline{\check{\mathcal{T}}(\omega,-2L+z,-z,\boldsymbol{x}_1,\boldsymbol{y}_3)}\Big]\\&\cdot\check{\chi}(\omega,\boldsymbol{y}_2)\overline{\check{\chi}(\omega,\boldsymbol{y}_1)}d\boldsymbol{y}_1d\boldsymbol{y}_2d\boldsymbol{y}_3d\boldsymbol{y}_4\\&=\iint\mathbb{E}\Big[\check{\mathcal{T}}(\omega,-2L+z,-z,\boldsymbol{x}_1-\boldsymbol{x},\boldsymbol{y}_1)\overline{\check{\mathcal{T}}(\omega,-2L+z,-z,\boldsymbol{x}_1,\boldsymbol{y}_1')}\Big]\\&\cdot\check{\Lambda}_{\mathrm{t}}^{+}(\omega,\boldsymbol{y}_1'-\boldsymbol{y}_1;\boldsymbol{y}_1',z)d\boldsymbol{y}_1d\boldsymbol{y}_2d\boldsymbol{y}_1d\boldsymbol{y}_1'.\end{aligned}\tag{B.3}$$

Again this can be written in terms of center and offset coordinates as

$$\begin{aligned}&\check{\mathcal{H}}_{\mathrm{t}}^{-}(\omega,-\boldsymbol{y};\boldsymbol{x}-\boldsymbol{y}/2,z,L)\\&=\iint\mathbb{E}\left[\check{\mathcal{T}}(\omega,-2L+z,-z,\boldsymbol{x}+\boldsymbol{y}/2,\boldsymbol{y}_1)\overline{\check{\mathcal{T}}(\omega,-2L+z,-z,\boldsymbol{x}-\boldsymbol{y}/2,\boldsymbol{y}_1')}\right]\\&\qquad\times\check{\Lambda}_{\mathrm{t}}^{+}(\omega,\boldsymbol{y}_1'-\boldsymbol{y}_1;\boldsymbol{y}_1',z)d\boldsymbol{y}_1d\boldsymbol{y}_1'\\&=(2\pi)^{-2d}\iint e^{i(\boldsymbol{\kappa}\cdot\boldsymbol{y}+\boldsymbol{\kappa}'\cdot(\boldsymbol{y}_1-\boldsymbol{y}_1'))}W_{\omega}^{\mathrm{T}}\left(2(L-z),\boldsymbol{x},\frac{\boldsymbol{y}_1+\boldsymbol{y}_1'}{2},\boldsymbol{\kappa},\boldsymbol{\kappa}'\right)\\&\qquad\times\check{\Lambda}_{\mathrm{t}}^{+}(\omega,\boldsymbol{y}_1'-\boldsymbol{y}_1;\boldsymbol{y}_1',z)d\boldsymbol{\kappa}d\boldsymbol{\kappa}'d\boldsymbol{y}_1d\boldsymbol{y}_1'.\end{aligned}$$

Using (7.1), we then get

$$\begin{aligned}
&\check{\mathcal{H}}_{\mathrm{t}}^{-}\left(\omega,-\boldsymbol{y};\boldsymbol{x}-\frac{\boldsymbol{y}}{2},z,L\right)\\
&=(2\pi)^{-3d}\iint e^{i(\boldsymbol{\kappa}\cdot\boldsymbol{y}+\boldsymbol{\kappa}'\cdot(\boldsymbol{y}_1-\boldsymbol{y}_1'))}e^{-i(\boldsymbol{\kappa}'+\boldsymbol{\kappa})\cdot\boldsymbol{a}-i((\boldsymbol{y}_1+\boldsymbol{y}_1')/2-\boldsymbol{x}+\frac{\boldsymbol{\kappa}}{\omega}z^*)\cdot\boldsymbol{b}}\\
&\qquad\times e^{\frac{\omega^2}{4}\int_0^{z^*}D(\boldsymbol{a}+\frac{\boldsymbol{b}}{\omega}z')-D(\boldsymbol{0})dz'}d\boldsymbol{a}d\boldsymbol{b}\check{\Lambda}_{\mathrm{t}}^{+}(\omega,\boldsymbol{y}_1'-\boldsymbol{y}_1;\boldsymbol{y}_1',z)d\boldsymbol{\kappa}d\boldsymbol{\kappa}'d\boldsymbol{y}_1d\boldsymbol{y}_1'\\
&=(2\pi)^{-3d}\iint e^{i\boldsymbol{\kappa}\cdot(\boldsymbol{y}-\boldsymbol{a}-\frac{z^*\boldsymbol{b}}{\omega})}e^{i\boldsymbol{\kappa}'\cdot(\boldsymbol{y}_1-\boldsymbol{y}_1'-\boldsymbol{a})}e^{-i(\frac{\boldsymbol{y}_1+\boldsymbol{y}_1'}{2}-\boldsymbol{x})\cdot\boldsymbol{b}}\\
&\qquad\times e^{\beta(\omega,z^*)\int_0^1 D_0(\frac{\boldsymbol{a}}{l}+\frac{\boldsymbol{b}z^*}{\omega l}\zeta)-D_0(\boldsymbol{0})d\zeta}d\boldsymbol{a}d\boldsymbol{b}\check{\Lambda}_{\mathrm{t}}^{+}(\omega,\boldsymbol{y}_1'-\boldsymbol{y}_1;\boldsymbol{y}_1',z)d\boldsymbol{\kappa}d\boldsymbol{\kappa}'d\boldsymbol{y}_1d\boldsymbol{y}_1'
\end{aligned}$$

for $z^*=2(L-z)$. Integrating in $\boldsymbol{\kappa}$ and $\boldsymbol{\kappa}'$ and evaluating the resulting two Dirac distributions, we find

$$\begin{aligned}
\check{\mathcal{H}}_{\mathrm{t}}^{-}\left(\omega,-\boldsymbol{y};\boldsymbol{x}-\frac{\boldsymbol{y}}{2},z,L\right)&=(2\pi)^{-d}\iint e^{-i\boldsymbol{b}\cdot(\boldsymbol{y}_1'+\boldsymbol{y}/2-\frac{z^*\boldsymbol{b}}{2\omega})}e^{i\boldsymbol{x}\cdot\boldsymbol{b}}\\
&\quad\times e^{\beta(\omega,z^*)\int_0^1 D_0(\frac{\boldsymbol{y}}{l}-\frac{\boldsymbol{b}z^*}{\omega l}\zeta)-D_0(\boldsymbol{0})d\zeta}d\boldsymbol{b}\check{\Lambda}_{\mathrm{t}}^{+}(\omega,-\boldsymbol{y}-z^*\boldsymbol{b}/\omega;\boldsymbol{y}_1',z)d\boldsymbol{y}_1d\boldsymbol{y}_1'.
\end{aligned}$$

Upon the change of variables $\boldsymbol{b}\mapsto-\boldsymbol{s}\omega l/z^*$, we get

$$\begin{aligned}
\check{\mathcal{H}}_{\mathrm{t}}^{-}\left(\omega,-\boldsymbol{y};\boldsymbol{x}-\frac{\boldsymbol{y}}{2},z,L\right)&=\frac{1}{(2\pi\alpha(\omega,z^*)l)^d}\iint e^{i\frac{\boldsymbol{s}\cdot(\boldsymbol{y}_1'+\boldsymbol{y}/2)}{l\alpha(\omega,z^*)}}e^{\frac{i|\boldsymbol{s}|^2}{2\alpha(\omega,z^*)}}e^{-\frac{i\boldsymbol{x}\cdot\boldsymbol{s}}{l\alpha(\omega,z^*)}}\\
&\quad\times e^{\beta(\omega,z^*)\int_0^1 D_0(\frac{\boldsymbol{y}}{l}+\boldsymbol{s}\zeta)-D_0(\boldsymbol{0})d\zeta}\check{\Lambda}_{\mathrm{t}}^{+}(\omega,-\boldsymbol{y}-l\boldsymbol{s};\boldsymbol{y}_1',z)d\boldsymbol{s}d\boldsymbol{y}_1'\\
&=\frac{1}{(2\pi l\alpha(\omega,z^*))^d}\iint e^{\frac{i|\boldsymbol{s}|^2}{2\alpha(\omega,z^*)}}e^{-\frac{i(\boldsymbol{x}-\boldsymbol{y}/2)\cdot\boldsymbol{s}}{l\alpha(\omega,z^*)}}\\
&\quad\times e^{\beta(\omega,z^*)\int_0^1 D_0(\frac{\boldsymbol{y}}{l}+\boldsymbol{s}\zeta)-D_0(\boldsymbol{0})d\zeta}\tilde{\Lambda}_{\mathrm{t}}^{+}\left(\omega,-\boldsymbol{y}-l\boldsymbol{s};\frac{\boldsymbol{s}}{l\alpha(\omega,z^*)},z\right)d\boldsymbol{s}. \qquad \text{(B.4)}
\end{aligned}$$

Then, by comparing with (B.2) and observing that $\alpha(\omega,z^*)=2\alpha(\omega,L-z)$, $\beta(\omega,z^*)=2\beta(\omega,L-z)$, we conclude $\check{\mathcal{H}}_{\mathrm{t}}^{-}(\omega,-\boldsymbol{y};\boldsymbol{x}-\boldsymbol{y}/2,z,L)=\check{\Lambda}_{\mathrm{t}}^{-}(\omega,-\boldsymbol{y};\boldsymbol{x}-\boldsymbol{y}/2,z,L)$. We therefore have

$$\begin{aligned}
&\check{\Lambda}_{\mathrm{t}}^{-}(\omega,\boldsymbol{x};\boldsymbol{x}_1,z,L)=\frac{1}{4}\iint\mathbb{E}\left[\check{\mathcal{T}}(\omega,-z,0,\boldsymbol{y}_4,\boldsymbol{y}_2)\overline{\check{\mathcal{T}}(\omega,-z,0,\boldsymbol{y}_3,\boldsymbol{y}_1)}\right]\\
&\quad\times\mathbb{E}\left[\check{\mathcal{R}}(\omega,-L,-z,\boldsymbol{x}_1-\boldsymbol{x},\boldsymbol{y}_4)\overline{\check{\mathcal{R}}(\omega,-L,-z,\boldsymbol{x}_1,\boldsymbol{y}_3)}\right]\check{\chi}(\omega,\boldsymbol{y}_2)\overline{\check{\chi}(\omega,\boldsymbol{y}_1)}d\boldsymbol{y}_1d\boldsymbol{y}_2d\boldsymbol{y}_3d\boldsymbol{y}_4\\
&=\frac{1}{4}\iint\mathbb{E}\left[\check{\mathcal{T}}(\omega,-z,0,\boldsymbol{y}_4,\boldsymbol{y}_2)\overline{\check{\mathcal{T}}(\omega,-z,0,\boldsymbol{y}_3,\boldsymbol{y}_1)}\right]\\
&\quad\times\mathbb{E}\left[\check{\mathcal{T}}(\omega,-2L+z,-z,\boldsymbol{x}_1-\boldsymbol{x},\boldsymbol{y}_4)\overline{\check{\mathcal{T}}(\omega,-2L+z,-z,\boldsymbol{x}_1,\boldsymbol{y}_3)}\right]\\
&\quad\times\check{\chi}(\omega,\boldsymbol{y}_2)\overline{\check{\chi}(\omega,\boldsymbol{y}_1)}d\boldsymbol{y}_1d\boldsymbol{y}_2d\boldsymbol{y}_3d\boldsymbol{y}_4\\
&=\frac{1}{4}\iint\mathbb{E}\left[\check{\mathcal{T}}(\omega,-2L+z,0,\boldsymbol{x}_1-\boldsymbol{x},\boldsymbol{y}_2)\overline{\check{\mathcal{T}}(\omega,-2L+z,0,\boldsymbol{x}_1,\boldsymbol{y}_1)}\right]\check{\chi}(\omega,\boldsymbol{y}_2)\overline{\check{\chi}(\omega,\boldsymbol{y}_1)}d\boldsymbol{y}_1d\boldsymbol{y}_2\\
&=\check{\Lambda}_{\mathrm{t}}^{+}(\omega,\boldsymbol{x};\boldsymbol{x}_1,2L-z).
\end{aligned}$$

Appendix C. Wigner asymptotics. We cast the Wigner distribution in a suitable dimensionless form and present an asymptotic approximation valid in the

regime driven by the scaling relation in Assumption 3. In this case we have $l \ll r_0$ and relatively rapid medium fluctuations. Moreover, we have $\omega l r_0 = \mathcal{O}(z)$, which means that diffractive effects are of order one at depth z. This scaling assumption is equivalent to

$$\alpha_0 = \frac{z}{\omega r_0^2} \ll \alpha_e = \frac{z}{\omega l r_0} = \mathcal{O}(1) \ll \alpha = \alpha(\omega, z) = \frac{z}{\omega l^2}.$$

The parameters $\alpha_0, \alpha_e, \alpha$ are inverse Fresnel numbers with the aperture corresponding respectively to the source aperture r_0, the effective aperture $\sqrt{l r_0}$, and the medium correlation length l. They describe the strength of the diffractive effects for respectively a homogeneous medium with source aperture r_0, a random medium with again source aperture r_0, and a homogeneous medium with source aperture l.

We consider the following Fourier transform V_ω^{R} of the Wigner distribution W_ω^{R}:

$$W_\omega^{\mathrm{R}}(z, \boldsymbol{x}, \boldsymbol{x}', \boldsymbol{\kappa}, \boldsymbol{\kappa}') = \frac{1}{(2\pi)^d} \int V_\omega^{\mathrm{R}}\Big(z, \frac{\boldsymbol{\kappa} + \boldsymbol{\kappa}'}{2}, \boldsymbol{\kappa} - \boldsymbol{\kappa}', \boldsymbol{\kappa}''\Big) e^{i\boldsymbol{\kappa}''\cdot(\boldsymbol{x}'-\boldsymbol{x})} d\boldsymbol{\kappa}'', \tag{C.1}$$

which we introduce because the stationary maps that we will identify in Lemma C.1, in the asymptotic regime $\alpha \to \infty$, have simple representations in this new frame. Note also that this ansatz incorporates the fact that W_ω^{R} does not depend on $\boldsymbol{x} + \boldsymbol{x}'$, only on $\boldsymbol{x} - \boldsymbol{x}'$, $\boldsymbol{\kappa}$, and $\boldsymbol{\kappa}'$, which follows from the statistical stationarity of the random medium. The Fourier-transformed operator $V_\omega^{\mathrm{R}}(z, \boldsymbol{\kappa}, \boldsymbol{\kappa}', \boldsymbol{\kappa}'')$ has the form

$$V_\omega^{\mathrm{R}}(z, \boldsymbol{\kappa}, \boldsymbol{\kappa}', \boldsymbol{\kappa}'') = (\pi l)^d e^{\frac{iz}{\omega}\boldsymbol{\kappa}'\cdot\boldsymbol{\kappa}''} \mathcal{V}^{\mathrm{R}}\Big(1, \boldsymbol{\kappa} l, \boldsymbol{\kappa}' l, \boldsymbol{\kappa}'' l; \alpha(\omega, z), \beta(\omega, z)\Big), \tag{C.2}$$

where $(\mathcal{V}^{\mathrm{R}}(\zeta, \boldsymbol{q}, \boldsymbol{r}, \boldsymbol{s}; \alpha, \beta))_{\zeta\in[0,1]}$ is the solution of the dimensionless system

$$\begin{aligned}
\frac{\partial \mathcal{V}^{\mathrm{R}}}{\partial \zeta} = \frac{\beta}{(2\pi)^d} \int \hat{D}_0(\boldsymbol{u}) \Bigg[& \mathcal{V}^{\mathrm{R}}\Big(\zeta, \boldsymbol{q} - \frac{1}{2}\boldsymbol{u}, \boldsymbol{r} - \boldsymbol{u}, \boldsymbol{s}\Big) e^{-i\alpha \boldsymbol{s}\cdot\boldsymbol{u}\zeta} \\
& + \mathcal{V}^{\mathrm{R}}\Big(\zeta, \boldsymbol{q} - \frac{1}{2}\boldsymbol{u}, \boldsymbol{r} + \boldsymbol{u}, \boldsymbol{s}\Big) e^{i\alpha \boldsymbol{s}\cdot\boldsymbol{u}\zeta} + \mathcal{V}^{\mathrm{R}}\Big(\zeta, \boldsymbol{q} - \frac{1}{2}\boldsymbol{u}, \boldsymbol{r}, \boldsymbol{s} - \boldsymbol{u}\Big) e^{-i\alpha \boldsymbol{r}\cdot\boldsymbol{u}\zeta} \\
& + \mathcal{V}^{\mathrm{R}}\Big(\zeta, \boldsymbol{q} - \frac{1}{2}\boldsymbol{u}, \boldsymbol{r}, \boldsymbol{s} + \boldsymbol{u}\Big) e^{i\alpha \boldsymbol{r}\cdot\boldsymbol{u}\zeta} - 2\mathcal{V}^{\mathrm{R}}\Big(\zeta, \boldsymbol{\kappa}, \boldsymbol{r}, \boldsymbol{s}\Big) \\
& - \mathcal{V}^{\mathrm{R}}\Big(\zeta, \boldsymbol{q} - \frac{1}{2}\boldsymbol{u}, \boldsymbol{r} - \boldsymbol{u}, \boldsymbol{s} + \boldsymbol{u}\Big) e^{i\alpha[(\boldsymbol{r}-\boldsymbol{s})\cdot\boldsymbol{u} - |\boldsymbol{u}|^2]\zeta} \\
& - \mathcal{V}^{\mathrm{R}}\Big(\zeta, \boldsymbol{q} - \frac{1}{2}\boldsymbol{u}, \boldsymbol{r} - \boldsymbol{u}, \boldsymbol{s} - \boldsymbol{u}\Big) e^{-i\alpha[(\boldsymbol{r}+\boldsymbol{s})\cdot\boldsymbol{u} + |\boldsymbol{u}|^2]\zeta} \Bigg] d\boldsymbol{u},
\end{aligned} \tag{C.3}$$

starting from $\mathcal{V}^{\mathrm{R}}(\zeta = 0, \boldsymbol{q}, \boldsymbol{r}, \boldsymbol{s}; \alpha, \beta) = \delta(\boldsymbol{q})$. Recall that $\alpha(\omega, z) = z/(\omega l^2)$ and $\beta(\omega, z) = \sigma^2\omega^2 l z/4$.

The rapid transverse variations regime is particularly interesting to study because W_ω^{R} has multiscale behavior. In (C.3) this regime gives rise to rapid phases, and this allows us to identify a simplified description, and the multiscale behavior strongly influences the correlations. The following lemma describes the asymptotic behavior of $\mathcal{V}^{\mathrm{R}}$ as $\alpha \to \infty$. The presence of singular layers at $\boldsymbol{r} = \boldsymbol{0}$ and at $\boldsymbol{s} = \boldsymbol{0}$ requires particular attention and is responsible, for instance, for the enhanced backscattering

phenomenon [11] (corresponding to part (3) in Lemma C.1). In general (part (1) in Lemma C.1) the intensity of the reflection operator decays exponentially according to the parameter $\beta D_0(\mathbf{0})$ corresponding to the total scattering cross section. This decay follows from a partial loss of coherence by random forward scattering. However, as articulated in parts (2) and (3) of the lemma below, the coupling of wave modes depends on the full medium auto-correlation function if we look at nearby specular reflection and/or small spatial offset frequencies. This coupling will be important in the analysis of the correlations in section 10. The following lemma is proved in [11].

LEMMA C.1.

(1) *For any* $\boldsymbol{r} \neq \mathbf{0}$, $\boldsymbol{s} \neq \mathbf{0}$,

$$\mathcal{V}^{\mathrm{R}}(\zeta, \boldsymbol{q}, \boldsymbol{r}, \boldsymbol{s}; \alpha, \beta) \overset{\alpha\to\infty}{\longrightarrow} \delta(\boldsymbol{q}) e^{-2\beta D_0(\mathbf{0})\zeta}. \tag{C.4}$$

(2) *For any* $\boldsymbol{s} \neq \mathbf{0}$, *we have* $\mathcal{V}^{\mathrm{R}}(\zeta, \boldsymbol{q}, \frac{\boldsymbol{r}}{\alpha}, \boldsymbol{s}; \alpha, \beta) \overset{\alpha\to\infty}{\longrightarrow} \mathcal{V}^{\mathrm{R}}_{\boldsymbol{r}}(\zeta, \boldsymbol{q}; \beta)$, *where* $\mathcal{V}^{\mathrm{R}}_{\boldsymbol{r}}(\zeta, \boldsymbol{q}; \beta)$ *is the solution of*

$$\frac{\partial \mathcal{V}^{\mathrm{R}}_{\boldsymbol{r}}}{\partial \zeta} = \frac{2\beta}{(2\pi)^d} \int \hat{D}_0(\boldsymbol{u}) \left[\mathcal{V}^{\mathrm{R}}_{\boldsymbol{r}}\Big(\zeta, \boldsymbol{q} - \frac{1}{2}\boldsymbol{u}\Big) \cos\big(\boldsymbol{r}\cdot\boldsymbol{u}\zeta\big) - \mathcal{V}^{\mathrm{R}}_{\boldsymbol{r}}\big(\zeta, \boldsymbol{q}\big) \right] d\boldsymbol{u} \tag{C.5}$$

and is given explicitly by

$$\mathcal{V}^{\mathrm{R}}_{\boldsymbol{r}}(\zeta, \boldsymbol{q}; \beta) = \frac{1}{(2\pi)^d} \int e^{-i\boldsymbol{q}\cdot\boldsymbol{u}} e^{\beta \int_0^\zeta D_0(\frac{\boldsymbol{u}}{2}+\boldsymbol{r}\zeta') + D_0(\frac{\boldsymbol{u}}{2}-\boldsymbol{r}\zeta') - 2D_0(\mathbf{0}) d\zeta'} d\boldsymbol{u}. \tag{C.6}$$

Similarly, for any $\boldsymbol{r} \neq \mathbf{0}$, *we have* $\mathcal{V}^{\mathrm{R}}\left(\zeta, \boldsymbol{q}, \boldsymbol{r}, \frac{\boldsymbol{s}}{\alpha}; \alpha, \beta\right) \overset{\alpha\to\infty}{\longrightarrow} \mathcal{V}^{\mathrm{R}}_{\boldsymbol{s}}(\zeta, \boldsymbol{q}; \beta)$.

(3) *For any* $\boldsymbol{r}$ *and* $\boldsymbol{s}$, *we have*

$$\mathcal{V}^{\mathrm{R}}\Big(\zeta, \boldsymbol{q}, \frac{\boldsymbol{r}}{\alpha}, \frac{\boldsymbol{s}}{\alpha}; \alpha, \beta\Big) \overset{\alpha\to\infty}{\longrightarrow} \mathcal{V}^{\mathrm{R}}_{\boldsymbol{r}}(\zeta, \boldsymbol{q}; \beta) + \mathcal{V}^{\mathrm{R}}_{\boldsymbol{s}}(\zeta, \boldsymbol{q}; \beta) - \delta(\boldsymbol{q}) e^{-2\beta D_0(\mathbf{0})\zeta}. \tag{C.7}$$

REFERENCES

[1] C. BARDOS, J. GARNIER, AND G. PAPANICOLAOU, *Identification of Green's function singularities by cross correlation of noisy signals*, Inverse Problems, 24 (2008), 015011.

[2] M. CAMPILLO AND A. PAUL, *Long-range correlations in the diffuse seismic coda*, Science, 299 (2003), pp. 547–549.

[3] J. F. CLAERBOUT, *Synthesis of a layered medium from its acoustic transmission response*, Geophys., 33 (1968), pp. 264–269.

[4] M. V. DE HOOP AND K. SØLNA, *Estimating a Green's function from "field-field" correlations in a random medium*, SIAM J. Appl. Math., 69 (2009), pp. 909–932.

[5] A. DERODE, E. LAROSE, M. TANTER, J. DE ROSNY, A. TOURIN, M. CAMPILLO, AND M. FINK, *Recovering the Green's function from field-field correlations in an open scattering medium*, J. Acoust. Soc. Amer., 113 (2003), pp. 2973–2976.

[6] D. DRAGANOV, K. WAPENAAR, W. MULDER, J. SINGER, AND A. VERDEL, *Retrieval of reflections from seismic background-noise measurements*, Geophys. Res. Lett., 34 (2007), L04305.

[7] T. L. DUVALL, S. M. JEFFERIES, J. W. HARVEY, AND A. POMERANTZ, *Time distance helioseismology*, Nature, 362 (1993), pp. 430–432.

[8] J.-P. FOUQUE, J. GARNIER, G. PAPANICOLAOU, AND K. SØLNA, *Wave Propagation and Time Reversal in Randomly Layered Media*, Springer, New York, 2007.

[9] J. GARNIER AND G. PAPANICOLAOU, *Correlation based virtual source imaging in strongly scattering random media*, Inverse Problems, 28 (2012), 075002.

[10] J. GARNIER AND G. PAPANICOLAOU, *Passive sensor imaging using cross correlations of noisy signals in a scattering medium*, SIAM J. Imaging Sci., 2 (2009), pp. 396–437.

[11] J. GARNIER AND K. SØLNA, *Coupled paraxial wave equations in random media in the white-noise regime*, Ann. Appl. Probab., 19 (2009), pp. 318–346.

[12] J. GARNIER AND K. SØLNA, *Scaling limits for wave pulse transmission and reflection operators*, Wave Motion, 2 (2009), pp. 122–143.

[13] P. Roux, K. G. Sabra, P. Gerstoft, W. A. Kuperman, and M. Fehler, *P-waves from cross-correlation of seismic noise*, Geophys. Res. Lett., 32 (2005), L19303.
[14] L. Ryzhik, G. Papanicolaou, and J. B. Keller, *Transport equations for elastic and other waves in random media*, Wave Motion, 24 (1996), pp. 327–370.
[15] F. Scherbaum, *Seismic imaging of the site response using micro-earthquake recordings. Part* II: *Application to the Swabian Jura, Southwest Germany, seismic network*, Bull. Seismol. Soc. Amer., 77 (1987), pp. 1924–1944.
[16] N. M. Shapiro and M. Campillo, *Emergence of broadband Rayleigh waves from correlations of the ambient seismic noise*, Geophys. Res. Lett., 31 (2004), L07614.
[17] N. M. Shapiro, M. Campillo, L. Stehly, and M. Ritzwoller, *High-resolution surface-wave tomography from ambient seismic noise*, Science, 307 (2005), pp. 1615–1618.
[18] R. Snieder, K. Wapenaar, and K. Larner, *Spurious multiples in seismic interferometry of primaries*, Geophys., 71 (2006), pp. SI111–SI124.
[19] T. Tonegawa, K. Nishida, T. Watanabe, and K. Shiomi, *Seismic interferometry of teleseismic S-wave coda for retrieval of body waves: An application to the Philippine Sea slab underneath the Japanese islands*, Geophys. J. Int., 178 (2009), pp. 1574–1586.
[20] B. A. van Tiggelen, *Green function retrieval and time reversal in a disordered world*, Phys. Rev. Lett., 91 (2003), 243904.
[21] I. Vasconcelos, R. Snieder, and H. Douma, *Representation theorems and Green's function retrieval for scattering in acoustic media*, Phys. Rev E, 80 (2009), 036605.
[22] K. Wapenaar, D. Draganov, R. Snieder, X. Campman, and A. Verdel, *Tutorial on seismic interferometry: Part* 1—*Basic principles and applications*, Geophys., 75 (2010), pp. 195–209.
[23] K. Wapenaar, E. Slob, and R. Snieder, *On seismic interferometry, the generalized optical theorem, and the scattering matrix of a point scatterer*, Geophys., 75 (2010), pp. SA27–SA34.
[24] K. Wapenaar, E. Slob, R. Snieder, and A. Curtis, *Tutorial on seismic interferometry: Part* 2—*Underlying theory and new advances*, Geophys., 75 (2010), pp. 211–227.
[25] K. Wapenaar and J. van der Neut, *A representation for Green's function by multidimensional deconvolution*, J. Acoust. Soc. Amer., 128 (2010), pp. 366–371.
[26] R. L. Weaver, *Ward identities and the retrieval of Green's functions in the correlations of a diffuse field*, Wave Motion, 45 (2008), pp. 596–604.
[27] R. L. Weaver and O. I. Lobkis, *Ultrasonics without a source: Thermal fluctuation correlations at MHz frequencies*, Phys. Rev. Lett., 93 (2001), 254301.
[28] H. Yao, R. D. van der Hilst, and M. V. de Hoop, *Surface-wave array tomography in SE Tibet from ambient seismic noise and two-station analysis*—I. *Phase velocity maps*, Geophys. J. Int., 166 (2006), pp. 732–744.